

# Spatial and temporal variability of the physical, carbonate and CO2 properties in the Southern Ocean surface waters during austral summer (2005-2019)

Margaux Brandon, Catherine Goyet, Franck Touratier, Nathalie Lefèvre, Élodie Kestenare, Rosemary Morrow

▶ **To cite this version:**

Margaux Brandon, Catherine Goyet, Franck Touratier, Nathalie Lefèvre, Élodie Kestenare, et al.. Spatial and temporal variability of the physical, carbonate and CO2 properties in the Southern Ocean surface waters during austral summer (2005-2019). Deep-sea research. Part A, Oceanographic research papers, 2022, 187, 10.1016/j.dsr.2022.103836 . insu-03778091

**HAL Id: insu-03778091**
**https://insu.hal.science/insu-03778091**

Submitted on 22 Sep 2022

**HAL** is a multi-disciplinary open access archive for the deposit and dissemination of scientific research documents, whether they are published or not. The documents may come from teaching and research institutions in France or abroad, or from public or private research centers.

L'archive ouverte pluridisciplinaire **HAL**, est destinée au dépôt et à la diffusion de documents scientifiques de niveau recherche, publiés ou non, émanant des établissements d'enseignement et de recherche français ou étrangers, des laboratoires publics ou privés.



Distributed under a Creative Commons Attribution - NonCommercial - NoDerivatives 4.0 International License

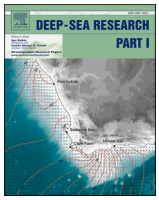
Deep–Sea Research I 187 (2022) 103836



Contents lists available at ScienceDirect

Deep-Sea Research Part I

journal homepage: www.elsevier.com/locate/dsri





# Spatial and temporal variability of the physical, carbonate and $CO_2$ properties in the Southern Ocean surface waters during austral summer (2005-2019)

Margaux Brandon [a,*], Catherine Goyet [b], Franck Touratier [b], Nathalie Lefèvre [a], Elodie Kestenare [c], Rosemary Morrow [c]

[a] IRD-LOCEAN-IPSL, Sorbonne Université/CNRS/MNHN, 4 Place Jussieu, 75005, Paris, France
[b] Laboratoire IMAGES-ESPACE-DEV, Univ. Perpignan Via Domitia, Perpignan, France
[c] LEGOS, CNRS/IRD/CNES/University of Toulouse III, Toulouse, France

ARTICLE INFO

*Keywords:*
Southern ocean
Sea surface temperature and salinity
Carbonate system
Air-sea $CO_2$ flux
Spatial variability
Temporal variability

ABSTRACT

In situ measurements of sea surface temperature (SST), salinity (SSS), Total Alkalinity ($A_T$) and Total Carbon ($C_T$) were obtained during austral summer (mid-February to mid-March) from 2005 to 2019 in the Southern Ocean (SO), along a transect between Hobart, Tasmania and Dumont d'Urville French Antarctic Station. The studied transect is divided in four regions from North to South: the Subtropical Zone (STZ), the Subantarctic Region (SAR), the Antarctic Region (AAR) and the Coastal Antarctic Zone (CAZ). Latitudinal distribution of measured SST, SSS, $A_T$, $C_T$ as well as calculated pH, $CO_2$ parameters (seawater fugacity of $CO_2$ ($fCO_{2sw}$), difference between seawater and atmospheric $fCO_2$ ($\Delta fCO_2$), $CO_2$ flux ($FCO_2$)) and satellite-derived Chlorophyll *a* (Chl-a) are discussed. We show that the variability of physical and carbonate parameters in the STZ and north of the SAR are related to the mesoscale activity. In the CAZ, the freshwater inputs from sea-ice melting strongly impact the variability of all parameters. The comparison between physical and carbonate parameters highlights that $A_T$ and $C_T$ are directly related to the latitudinal variability of SST and SSS. Study of the $CO_2$ parameters shows that the transect is a sink of $CO_2$ during February and March, with a mean $FCO_2$ of $-4.0 \pm 2.8$ mmol $m^{-2}$ $d^{-1}$. The most negative values of $FCO_2$ are found in the STZ and SAR north of 50°S and in the AAR south of 62°S, where biological activity is high. New simple empirical relationships are developed for $A_T$ from SST and SSS and for $C_T$ using SST, SSS and atmospheric $fCO_2$ ($fCO_{2atm}$) for the austral summer in the studied area. Using high resolution SSS and SST from the SURVOSTRAL program, trends of $A_T$ and $C_T$ are determined in the SAR and the AAR from 2005 to 2019. SST, SSS and $A_T$ increase over this period in the SAR, which might be explained by the southward migration of the Subtropical Front. In the AAR, no clear trend is detected. $C_T$ increases by $1.0 \pm 0.2$ and $0.8 \pm 0.3$ µmol $kg^{-1}$ $yr^{-1}$ in the SAR and AAR respectively. The trend in the AAR is attributed to the increase in anthropogenic $CO_2$ emissions in the atmosphere while, in the SAR, hydrographic changes also contribute to the increase. Using the coefficient associated with $fCO_{2atm}$ in the equation of $C_T$, we estimate the impact of atmospheric $CO_2$ increase on $C_T$ at $1.18 \pm 0.14$ µmol $kg^{-1}$ $yr^{-1}$ and $1.07 \pm 0.13$ µmol $kg^{-1}$ $yr^{-1}$ in the SAR and AAR respectively. Decreases in pH are observed in both regions ($-0.0018 \pm 0.0001$ and $-0.0026 \pm 0.0003$ $yr^{-1}$ in the SAR and AAR respectively), indicating the sensitivity of surface waters in the area towards the development of ocean acidification processes under rising anthropogenic emissions.

## 1. Introduction

Since the pre-industrial period, the atmospheric $CO_2$ has increased rapidly due to increasing human activities. Up to a quarter of these anthropogenic $CO_2$ emissions have been absorbed by the global ocean since then (Sabine et al., 2004; DeVries, 2014), with increasing uptake over the past decades (Gruber et al., 2019a, 2019b; Friedlingstein et al., 2020). But this uptake has consequences on the biogeochemistry of the ocean.

Over the past decades, increasing number of studies focused on the

* Corresponding author.
*E-mail address:* margaux.brandon@locean.ipsl.fr (M. Brandon).

https://doi.org/10.1016/j.dsr.2022.103836
Received 13 December 2021; Received in revised form 8 July 2022; Accepted 14 July 2022
Available online 19 July 2022
0967-0637/© 2022 The Authors. Published by Elsevier Ltd. This is an open access article under the CC BY-NC-ND license (http://creativecommons.org/licenses/by-nc-nd/4.0/).

changes in the physical, carbonate and $CO_2$ system to better constrain the impact of anthropogenic carbon ($C_{ant}$) on the global ocean. Under increasing atmospheric $CO_2$ concentration, $C_T$ inventory has changed. Gruber et al. (2019a) estimated a total $C_{ant}$ inventory of 34.4 PgC (petagrams of carbon) between 1994 and 2007 in the global ocean. In surface waters, $C_T$ presents an increase around $1 \pm 0.6$ μmol $kg^{-1}$ $yr^{-1}$ in different regions of the ocean (Bates et al., 2014; Takahashi et al., 2014; Lauvset et al., 2015; Merlivat et al., 2018; Lo Monaco et al., 2021; Gregor and Gruber, 2021), in part linked with the uptake of $C_{ant}$. In the intermediate and deep waters, storage of $C_{ant}$ has also been observed, with strong spatial variability (Gruber et al., 2009, 2019a; Murata et al., 2010; Peng and Wanninkhof, 2010; Mahieu et al., 2020). As a consequence of the accumulation of $C_{ant}$ in the ocean, pH has decreased by 0.1 since the beginning of the industrial era, leading to ocean acidification (Orr et al., 2005; Doney et al., 2009; Bates et al., 2014; Jiang et al., 2019).

The Southern Ocean (SO) is the key region in terms of $C_{ant}$ uptake, accounting for 40% of the global ocean anthropogenic $CO_2$ absorption (Sabine et al., 2004; Mikaloff Fletcher et al., 2006; DeVries, 2014). At the surface, the waters unsaturated in $CO_2$ with respect to the atmosphere enhance the uptake of $CO_2$, while the intermediate and bottom-water formation in this region favours the export and storage of $C_{ant}$ at depth (Gruber et al., 2009; DeVries, 2014). Moreover, the cold surface waters at high latitudes increase the solubility of $CO_2$, favouring the $CO_2$ uptake compared to warmer waters.

The understanding of the carbon cycle dynamics and the impact on the uptake of $C_{ant}$ requires a good spatial and temporal coverage of in-situ data in the ocean, combining multiple parameters of the carbonate system, such as $C_T$, $A_T$, pH and $CO_2$ fluxes. Strong efforts have been made to increase these datasets, in particular measurements of surface waters fugacity of $CO_2$ ($fCO_{2sw}$), allowing us to quantify the $CO_2$ fluxes ($FCO_2$) between the ocean and the atmosphere. Most of these observations are based on spring and summer cruises. They have revealed a strong sink of $CO_2$ during summer in the SO, with mean $FCO_2$ around $-3$ mmol $m^{-2}$ $d^{-1}$ (Metzl et al., 1995; Brévière et al., 2006; Gray et al., 2018). The most important sinks are located in the Subantarctic Zone, Polar Front Zone and Seasonal Ice-free Zone during summer, with $FCO_2$ values down to $-20$ mmol $m^{-2}$ $d^{-1}$, and are associated with high biological activity in the surface waters (Metzl et al., 1999; Brévière et al., 2006; Gruber et al., 2009, 2019b; Gray et al., 2018). In contrast, the few studies available based on winter cruises or autonomous observation platforms have determined that this oceanic region was a source of $CO_2$ during winter, with $FCO_2$ values around 1 mmol $m^{-2}$ $d^{-1}$ (Metzl et al., 1995, 1999, 2006; Gray et al., 2018). When focusing on longer timescales, $fCO_{2sw}$ observations show an increasing rate similar to that of the atmospheric $fCO_2$ ($fCO_{2atm}$) (~2 μatm $yr^{-1}$) (Metzl, 2009; Takahashi et al., 2009; Munro et al., 2015; Lauvset et al., 2015; Xue et al., 2018; Leseurre et al., 2022), even as the $CO_2$ uptake by the SO has been fluctuating over the past decades (Le Quéré et al., 2007; Lovenduski et al., 2008; Lenton et al., 2013; Landschützer et al., 2015). The observed increase in $C_{ant}$ in the SO drives the acidification of surface waters, with a decrease in pH quantified around $-0.002 \pm 0.001$ $yr^{-1}$ (Midorikawa et al., 2012; Takahashi et al., 2014; Munro et al., 2015; Lauvset et al., 2015; Williams et al., 2015; Xue et al., 2018; Leseurre et al., 2022).

In the meantime, temperature and salinity observations are recording changes in heat content and oceanic circulation in the SO. Recent studies on the decadal evolution of temperature in the SO highlighted a warming of Subantarctic Surface and Intermediate Waters of around 0.2–0.3 °C per decade, while south of the Polar Front, the trend in SST is less clear, with small changes in the Antarctic Zone and a cooling of surface waters in the sea-ice zone in eastern Antarctica (Armour et al., 2016; Sallée, 2018; Auger et al., 2021). At the scale of the whole SO, SSS observations over past decades show different trends. While some studies present a freshening of surface waters (Durack and Wijffels 2010; Durack et al., 2012; de Lavergne et al., 2014), others show no significant trend (Midorokawa et al., 2012; Takahashi et al., 2014; Morrow and Kestenare, 2014). However, variations in westerly wind intensity, sea-ice concentration and gyre location have been observed in the past decades, with possible impact on the SSS as well as SST, and to a bigger scale, on SO circulation (Böning et al., 2008; de Lavergne et al., 2014; Haumann et al., 2016; Morrow and Kestenare, 2017; Yang et al., 2020).

Despite the increasing amount of surface observations, data resolution is still sparse (Bakker et al., 2016; Gray et al., 2018). In particular, direct in situ measurements of $A_T$ and $C_T$ are scarce (Metzl et al., 2006; Laika et al., 2009; Midorikawa et al., 2012; Leseurre et al., 2022). The few estimated trends of $A_T$ in the SO are often not significant or show important errors (Lenton et al., 2012; Midorikawa et al., 2012; Takahashi et al., 2014; Xue et al., 2018). On the opposite, all studies agree on an increase in $C_T$ in all regions of the SO, with rates around $0.7 \pm 0.3$ μmol $kg^{-1}$ $yr^{-1}$ (Lenton et al., 2012; Takahashi et al., 2014; Xue et al., 2018; Leseurre et al., 2022). This lack of observation limits the understanding of spatial distribution and temporal evolution of the carbonate system. Empirical relationships of $A_T$ and $C_T$ using SST and SSS are often used to complete the data coverage when no in situ measurements of the carbonate parameters are available (Lee et al., 2000, 2006). Previous studies have defined the equations of $A_T$ and $C_T$ in the SO, but these equations have been determined over the entire SO or are limited to a few cruises (Metzl et al., 1999; Lee et al., 2000, 2006; Laika et al., 2009).

Here we present the latitudinal distribution and decadal evolution of SST, SSS and carbonate parameters ($A_T$, $C_T$, pH, $fCO_{2sw}$, $\Delta fCO_2$ - the difference between seawater and atmospheric fugacity, and $FCO_2$) along a transect south of Tasmania during austral summer (mid-February to mid-March) for the period 2005–2019. In order to complete our dataset, new simple empirical relationships of $A_T$ and $C_T$ are determined based on SSS and SST measurements and are compared with equations previously published in the SO. Temporal evolution of physical and carbonate parameters are investigated from 2005 to 2019. Finally, we discuss the impact of increasing $C_{ant}$ uptake on the $C_T$ inventory and on ocean acidification.

## 2. Material and methods

### 2.1. Data collection and satellite observations

In situ measurements of SST, SSS, $A_T$ and $C_T$ were obtained onboard RV *L'Astrolabe* between Hobart, Tasmania (43°S, 147°E) and Dumont d'Urville, Antarctica (67°S, 140°E) (Fig. 1) in austral summer (mid-February to mid-March) over the period 2005–2019 (Table 1). Continuous underway thermosalinograph measurements (SST, SSS) are part of the SURVOSTRAL program since 1993, and data used in this study cover the return trip during the entire period spanned by available $A_T$ and $C_T$ data between 2005 and 2019. Transects located too far away from the mean route were not considered. A total of 27 transects over 15 years were used for this study (https://sss.sedoo.fr, see Alory et al., 2015). These data were obtained at around 5 m depth every 1 min. The SSS accuracy is estimated to be between 0.005 and 0.01 (Morrow and Kestenare, 2014).

$A_T$ and $C_T$ were measured directly as part of the MINERVE program (https://campagnes.flotteoceanographique.fr/series/128/fr/), that aims to better understand the interannual variability of ocean-atmosphere $CO_2$ fluxes in the SO south of Tasmania. The data were collected between 2005 and 2019 but because of measurement accuracy issues, some transects were not used in this study, leading to a total of 9 cruises selected. For each $A_T$ and $C_T$ measurement, the closest SST and SSS measurements from SURVOSTRAL were chosen.

$A_T$ and $C_T$ were measured from surface waters (at 5 m depth) every 25 min for the cruises from 2005 to 2010 and every 2 h for 2019. Measurements were performed using a potentiometric method using a closed cell (Goyet et al., 1991). Until 2010, measurements were made using a fully automated system maintained at $18.0 \pm 0.1$ °C. The precision of $A_T$ and $C_T$ were estimated at 3.5 and 2.7 μmol $kg^{-1}$,

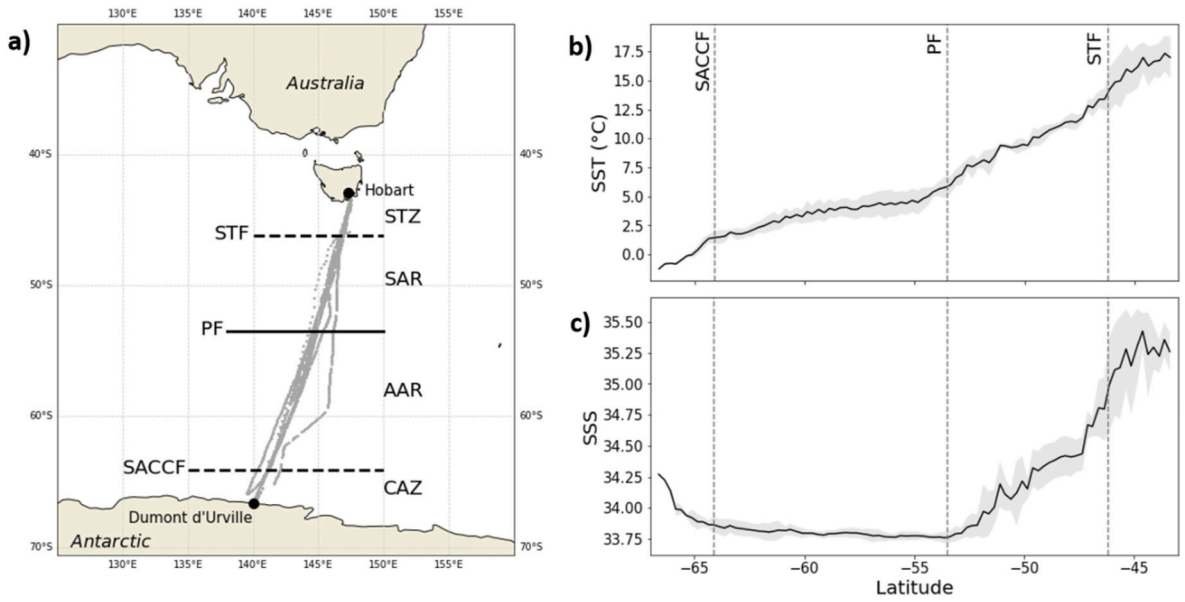



**Fig. 1. a)** Location of transects (grey lines) between Hobart, Tasmania and Dumont d'Urville, Antarctic. Oceanographic fronts and studied regions are located. STZ: Subtropical Zone, SAR: Subantarctic Region, AAR: Antarctic Region, CAZ: Coastal Antarctic Zone, STF: Subtropical Front, PF: Polar Front, SACCF: Southern Antarctic Circumpolar Current Front. **b)** Latitudinal variation of Sea Surface Temperature (SST) and c) Salinity (SSS) from 2005 to 2019 collected at the same time as $A_T$ and $C_T$. SST and SSS data have been averaged on 0.25° latitude bins. The black curve represents the mean value and the shaded grey area corresponds to one standard deviation.

**Table 1**
Cruises of the RV L'Astrolabe used in this study from the SURVOSTRAL program and availability of $A_T$ and $C_T$ measurements from the MINERVE program (HOB-DDU define data for the outward cruise and DDU-HOB for the return cruise).

| year | Hobart-Dumont d'Urville | Dumont d'Urville-Hobart | Measured $A_T$ and $C_T$ |
|---|---|---|---|
| 2005 | 18–23 Feb | 26 Feb - 3 Mar | HOB-DDU, DDU-HOB |
| 2006 | 17–22 Feb | 25 Feb - 2 Mar | |
| 2007 | 18–23 Feb | 27 Feb - 4 Mar | DDU-HOB |
| 2008 | 18–23 Feb | 27 Feb - 2 Mar | HOB-DDU, DDU-HOB |
| 2009 | 18–23 Feb | 27 Feb - 4 Mar | DDU-HOB |
| 2010 | 19–23 Feb | 28 Feb - 5 Mar | HOB-DDU, DDU-HOB |
| 2011 | 21–25 Feb | 1–6 Mar | |
| 2012 | | 2–6 Mar | |
| 2013 | 20–25 Feb | 27 Feb - 4 Mar | |
| 2014 | 1–6 Mar | 12–16 Mar | |
| 2015 | | 14–18 Mar | |
| 2016 | | 1–5 Mar | |
| 2017 | 23–28 Feb | 2–7 Mar | |
| 2018 | 20–24 Feb | 28 Feb - 4 Mar | |
| 2019 | 13–18 Feb | 22–26 Feb | HOB-DDU |

respectively. For 2019, discrete measurements were performed at IMAGES-ESPACE-DEV, Perpignan. The final dataset used for this study contains more than 188 000 measurements of in situ SST and SSS, and a total of 1755 observations of $A_T$, $C_T$.

Biological activity along the section was estimated for February and March of each year using 8-day composites of MODIS Aqua satellite images of Chlorophyll *a* (Chl-a) concentration at 4 km resolution, over the weeks covered by the cruises. Only data within a range of ±3° of longitude from the mean transect were selected and were zonally averaged for each available latitude.

### 2.2. Region determination and hydrographic fronts location

The SO is divided into multiple regions and zones, delimited by hydrographic fronts (Orsi et al., 1995). These fronts are determined by strong temperature and salinity gradients. Based on the definitions of surface frontal signatures from Chaigneau and Morrow (2002), the dataset was divided in four regions: The Subtropical Zone (STZ), north of the Subtropical Front (STF); The Subantarctic Region (SAR), between the STF and the Polar Front (PF); the Antarctic Region (AAR), between the PF and the Southern Antarctic Circumpolar Current Front (SACCF); and the Coastal Antarctic Zone (CAZ), south of the SACCF down to the Antarctic coast (Fig. 1).

Using continuous SURVOSTRAL SST and SSS data for each cruise, we determined the mean position of each front along the transect. The STF is located around 46.2°S when SSS displays a strong gradient and SST shows a significant rapid decrease in latitude. The PF is defined as the northern limit of constant SSS of ~33.75 as well as a change in the slope of SST, its mean position is located along our sections at around 53.5°S. The position of the SACCF is delimited by the decrease in SST and the increase in SSS at around 64.1°S. Within the SAR, the Subantarctic Front, defined with a gradient of SST and SSS around 49–52°S, divides the region into two zones, the Subantarctic Zone to the north and the Polar Front Zone to the south. This is the strongest subsurface front in the region and highly variable with strong mesoscale energy, yet on average, the mean surface characteristics of SST and SSS gradients are weaker (Fig. 1), so this front was not considered and the two zones were merged into the SAR. The same choice was made for the other weaker surface fronts associated with the Antarctic Circumpolar Current.

### 2.3. Determination of $A_T$ and $C_T$ from empirical relationships

In order to complete the dataset and have a better understanding of the long-term evolution of $A_T$ and $C_T$, the carbonate parameters were calculated using relevant parameters affecting their variability.

The relationships were determined using TableCurve 3D software. Different equations forms (polynomial, logarithmic, exponential) were tested for the relationships. The simplest relationships with the best fit with measured data were chosen. Equations with associated coefficient and standard error are presented and are compared with existing ones in the Results and Discussion section.

### 2.4. Air-sea $CO_2$ flux

The $fCO_{2sw}$ was calculated with $CO_2$SYS software (Lewis and Wallace, 1998) for Python (PyCO$_2$SYS 1.6, Humphreys et al., 2022) using in situ measurements of SST, SSS, $A_T$ and $C_T$ as well as mean silicate and phosphate concentration for February and March of the World Ocean Atlas 2018 dataset (Garcia et al., 2019). Dissociation constants defined by Mehrbach et al. (1973) and refitted by Dickson and Millero (1987) as well as $KHSO_4$ dissociation constant from Dickson (1990) were used for the calculation. In order to complete the carbonate parameters, pH was also determined using PyCO$_2$SYS.

The $fCO_{2atm}$ was obtained from monthly $xCO_2$ measurements from Cape Grim, Tasmania (https://gml.noaa.gov/dv/data/https://www.csiro.au/greenhouse-gases/), converted into $fCO_{2atm}$ at 100% humidity using monthly mean atmospheric pressure of the NCEP/NCAR reanalysis project at 2.5° × 2.5° grid and linearly interpolated at the position of each measurement along the transect (Data provided by the NOAA Physical Sciences Laboratory, Boulder, Colorado, USA, from their website at https://psl.noaa.gov/data/gridded/data.ncep.reanalysis.html).

The $FCO_2$ was calculated using the following approximate formula (neglecting the skin effect):

$$FCO_2 = k\, S_O(fCO_{2sw} - fCO_{2atm}) \quad (1)$$

where $S_O$ the solubility of seawater $CO_2$ of Weiss (1974) and k, the gas transfer velocity, calculated using the formula of Wanninkhof (2014):

$$k = 0.251 U_{10}^2 \left(\frac{Sc}{660}\right)^{-0.5} \quad (2)$$

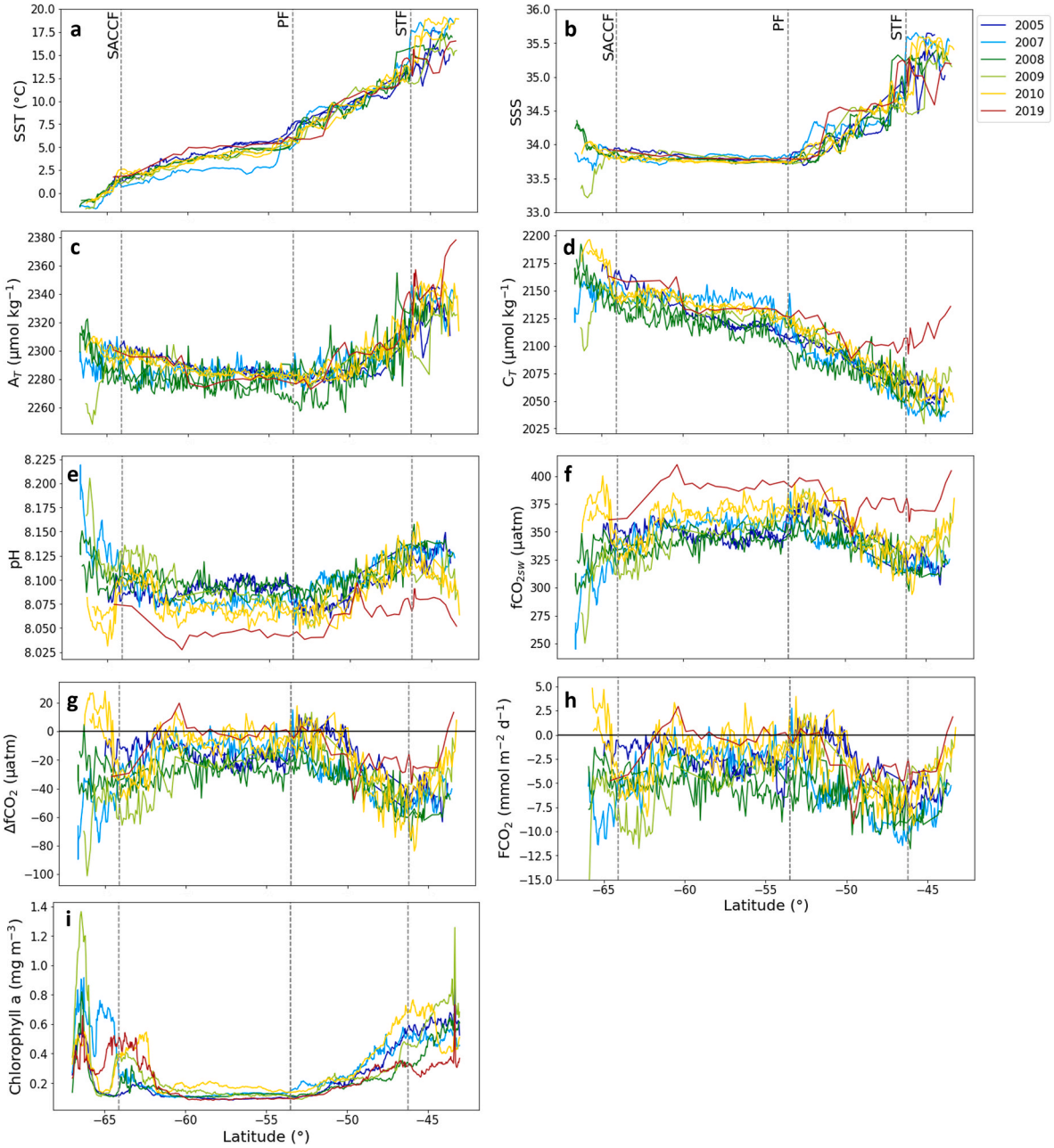



**Fig. 2.** Latitudinal variations of a) SST, b) SSS), c) $A_T$, d) $C_T$, e) pH, f) calculated $fCO_{2sw}$, g) $\Delta fCO_2$, h) $FCO_2$ and i) MODIS Aqua satellite observation of mean Chl-a for February and March between 2005 and 2019, for the years when $A_T$ and $C_T$ measurements are available. Dotted lines indicate the location of the fronts, from north to south: Subtropical Front (STF), Polar Front (PF) and Southern Antarctic Circumpolar Current Front (SACCF).

where $U_{10}$ is the wind speed at 10 m above sea level and Sc, the Schmidt number.

The monthly mean wind speed was taken from the Remote Sensing Systems website (Wentz et al., 2015; https://remss.com/measurements/wind/) and was co-located at each measurement location.

## 3. Results and Discussion

### 3.1. Latitudinal distribution of surface physical, carbonate and $CO_2$ parameters between Hobart and Dumont d'Urville

We first present the latitudinal distribution of physical (SST, SSS), carbonate ($A_T$, $C_T$, pH) and $CO_2$ parameters ($fCO_{2sw}$, $\Delta fCO_2$ - the difference between seawater and atmospheric $fCO_2$, and $FCO_2$) as well as Chl-a satellite data along the transect for the period 2005–2019. We also discuss the relation between measured physical and carbonate parameters.

#### 3.1.1. SST and SSS

SST shows a southward decrease from 16.12 ± 1.89 °C in the STZ to −0.10 ± 1.06 °C in the CAZ (Fig. 2a). As described in the methodology section, SST presents strong gradients at the position of hydrographical fronts, leading to a non-linear cooling of surface waters along the transect. During the 2007 cruise, mean SST in the AAR is 1.41 °C cooler than the mean of other years. South of Tasmania, the fronts associated with the ACC are constrained by the Southeast Indian Ridge topography and form a quasi-permanent meander extending northward at around 145°E that brings colder waters up to 55°S of latitude (Sokolov and Rintoul, 2002; Park et al., 2019). The observed SST anomaly during 2007 can be explained by the eastward location of the cruise compared to all other cruises, and therefore crossing the meander formed with colder waters, highlighting the strong spatial variability of the fronts. SSS also shows a southward decrease from 35.27 ± 0.29 in the STZ to a value of 33.78 ± 0.05 at the PF (Fig. 2b). Surface waters in the STZ and the northern part of the SAR along the transect are influenced by the southward transport of subtropical warm and salty waters, originating from the Tasman Sea and carried by the East Australian Current (EAC) and Tasman Outflow to the East and by the Zeehan Current (ZC) to the West (Cresswell, 2000; Ridgway, 2007; Herraiz-Borreguero and Rintoul, 2010, 2011; Morrow and Kestenare, 2014; Pardo et al., 2017). Both SST and SSS present strong mesoscale and interannual variability in the STZ and also in the SAR. This variability can originate from two mechanisms. First, variations in the strength of the ZC and the EAC have been linked to large-scale changes in wind stress that impact on the southward transport of subtropical waters (Cai et al., 2005; Oliver et al., 2016; Oliver and Holbrook, 2018). The other mechanism that contributes to this variability is the presence of energetic mesoscale eddies and meanders along the STF and SAF (Chaigneau et al., 2004; Sokolov and Rintoul, 2009; Herraiz-Borreguero and Rintoul, 2011; Morrow and Kestenare, 2014). Previous studies in the region also highlighted the presence of cold-cores or cyclonic eddies originating from a meander (Morrow et al., 2004; Moreau et al., 2017). In our case, the local drops in SST and SSS observed in the STZ during 2005 and 2019 cruises could be explained by the northward migration of a cyclonic eddies formed south of the SAF.

In the AAR, the salinity is quite stable, showing only a 0.09 ± 0.05 increase from north to south of the region, with little variability. As described by Chaigneau and Morrow (2002) and Chaigneau et al. (2004), the layer of near-constant salinity at the surface of this region can be explained by strong Ekman and geostrophic currents, that transport freshwater from sea-ice melt in a north-eastward direction during spring and summer.

Finally, in the CAZ, SST rapidly decreases towards negative values whereas SSS shows strong variability, with values ranging between 33.21 and 34.35. While SSS drops drastically to 33.62 and 33.21 during the 2007 and 2009 cruises, respectively, we observe an increase in SSS in 2008. The SSS close to the coasts of Antarctica is strongly influenced by the formation and melting of sea-ice through the year and the lateral advection of sea-ice along the coast (Morrow and Kestenare, 2017). The peak in freshwaters recorded during summer in the CAZ are the consequence of late sea-ice melting, while the increase in SSS observed in 2008 may reflect less sea-ice and the presence of saltier shelf waters near the coast of Antarctica, or early sea-ice formation during late summer linked with brine rejection (Chaigneau and Morrow, 2002). The annual SSS measurements from SURVOSTRAL over 2005–2019 clearly shows the strong interannual variability depending on sea-ice melting and formation (Supplementary Fig. 1).

#### 3.1.2. Carbonate parameters ($A_T$, $C_T$, pH)

The highest $A_T$ values (mean 2331.2 μmol $kg^{-1}$) are recorded in the STZ before decreasing along the transect to reach a mean of 2279.4 ± 8.3 μmol $kg^{-1}$ at the PF (Fig. 2c). In the AAR, $A_T$ slightly increase southward from 2279.8 ± 6.8 to 2293.1 ± 8.7 μmol $kg^{-1}$. In the CAZ, $A_T$ shows strong variability, with mean value of 2294.4 ± 12.6 μmol $kg^{-1}$ and a minimum of 2248.0 μmol $kg^{-1}$ in 2009. Through the transect, $A_T$ latitudinal distribution strongly resembles that of SSS, emphasizing that $A_T$ variability is governed by the same factors impacting salinity (Fig. 3b). Indeed, In the surface ocean, $A_T$ is dependent on salinity changes through freshwater inputs and removal (precipitation-evaporation, sea-ice melting-formation), contributing to more than 80% of $A_T$ variability (Millero et al., 1998; Fry et al., 2015). However, when looking at the SSS-$A_T$ diagram (Fig. 3b), a linear relationship is only observed north of the PF and during episodes of freshening of surface waters in the CAZ. South of the PF, $A_T$ is inversely related to changes in SST (Fig. 3a). This relationship can be explained by the presence of upwelling of cold and AT-rich waters in the high latitudes of the SO (Millero et al., 1998; Key et al., 2004; Fry et al., 2015; Fine et al., 2017). The only exception to the SST-$A_T$ relationship south of the PF is in the CAZ, when strong freshening of surface waters impact $A_T$, while SST does not register any major change. In the STZ and SAR, the strong variability observed in the physical parameters seems to have a moderate impact on $A_T$. However, some intense events such as the rapid drop in SST and SSS at 45°S during 2005 cruise, lead to strong variability in $A_T$ – in this case, a decrease in $A_T$ of around 25 μmol $kg^{-1}$. This highlights the importance of both SSS and SST in the variability of $A_T$.

$C_T$ presents a mean southward increase from 2058.9 ± 13.9 μmol $kg^{-1}$ in the STZ to 2156.3 ± 19.4 μmol $kg^{-1}$ in the CAZ (Fig. 2d). However, the rise in $C_T$ is not linear and changes of slope can be observed at the position of the fronts. The latitudinal distribution of $C_T$ is inversely related to the one of SST, as shown by the linear negative relationship observed on the SST-$C_T$ diagram (Fig. 3c). The poleward rise observed in $C_T$ concentration is influenced by the decrease in SST, leading to an increase in solubility of $CO_2$ at the ocean surface, but also, to a smaller extent, by the upwelling of $C_T$-rich waters south of the Polar Front (Wu et al., 2019 and references therein). Like $A_T$, no relationship is observed between SSS and $C_T$ south of the PF (Fig. 3d). North of the PF, however, a negative relationship is observed between both parameters. During episodes of surface waters freshening in the CAZ, $C_T$ is also affected by the decrease in SSS. Because the SST is only slightly affected by these events, we observe no clear relationship between SST and $C_T$ during these events, as seen for $A_T$.

Besides changes in solubility and evaporation/precipitation, surface $C_T$ is also influenced by biological processes (primary production, calcification). Increase in biological activity at the surface ocean would decrease the $C_T$, as seen off the South-East coast of Madagascar in 2020 (Metzl et al., 2022). Along the studied transect, satellite images show higher Chl-a concentration north of 51°S and south of 62°S (Fig. 2i). However, the concentrations stay quite low and no clear decrease in $C_T$ are observed at the same locations.

Finally, surface $C_T$ is also modulated by the difference in $fCO_2$ between the atmosphere and the surface ocean. Because of the increase in anthropogenic emissions, variations in $C_T$ are not only from natural

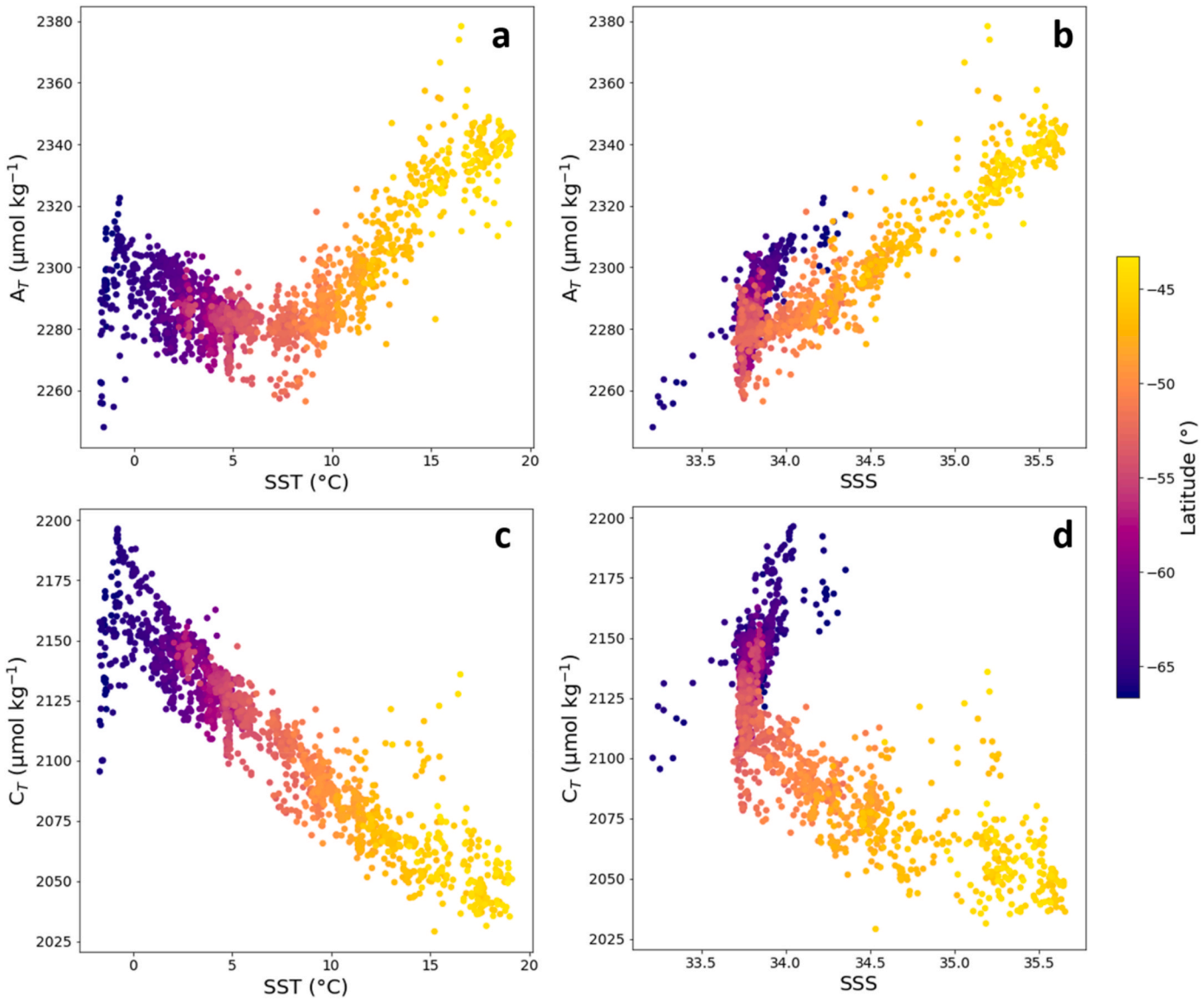



**Fig. 3.** Relationship between physical and carbonate parameters depending on latitude along the Hobart-Dumont d'Urville transect. a) SST-$A_T$, b) SSS-$A_T$, c) SST-$C_T$, d) SSS-$C_T$.

origin but also from anthropogenic origin ($C_{ant}$). While $C_T$ can be measured in-situ, $C_{ant}$ cannot be measured directly. Multiple approaches using carbonate system parameters have been carried out over these past decades to quantify the uptake and storage of $C_{ant}$ by the ocean below the surface and to identify the oceanic regions of importance for the sink of $CO_2$ and $C_{ant}$ (Chen, 1982, 1993; Coatanoan et al., 2001; Gruber et al., 2009; Sabine and Tanhua, 2010 and references therein). But because of the complexity of the spatial and temporal variability of physical and biological processes occurring in the surface layer, the part of surface $C_T$ from anthropogenic origin is difficult to differentiate from $C_T$ of natural origin. The evolution of $C_T$ in a context of increasing anthropogenic emission will be discussed in the last chapter.

In 2019, higher $C_T$ is observed in the STZ and north of the SAR, with a mean value of 40.3 ± 3.8 µmol kg$^{-1}$ higher compared to the mean of cruises between 2005 and 2010. Several factors could explain this major shift in $C_T$ concentration. First, surface waters are affected by the increasing uptake of $C_{ant}$. In particular, subtropical and subantarctic waters have high anthropogenic $CO_2$ concentrations (Sabine et al., 2004; Carroll et al., 2022), and over the past decades, an accumulation of $C_{ant}$ in the upper water-column has been registered north of 50°S along a transect close to this study (Carter et al., 2019). A part of the increase in $C_T$ observed in 2019 could therefore originate from rising $C_{ant}$ in surface waters. Then, because of the strong mesoscale activity in this region, a part of this increase could also be related to the presence of a cyclonic eddy along the cruise transect. Indeed, Moreau et al. (2017) showed that the inner surface waters had higher $C_T$ concentrations compared to waters outside the eddy. Finally, lower biological activity could also act to increase the mean surface $C_T$ concentrations in this region, as seen in Fig. 2i.

Surface pH, calculated using measured physical and carbonate parameters, ranges between 8.028 and 8.219 (Fig. 2e). The highest values are located around the STF and in the CAZ. Strong variability in pH is observed in this latter zone, with a maximum difference of 0.188. 2019 values are clearly lower than during years 2005–2019. This trend will be further discussed in the last section of the discussion.

### 3.1.3. *Air-sea $CO_2$ exchanges and biological activity*

$fCO_{2sw}$ ranges between 245.0 and 410.1 µatm and the latitudinal distribution shows strong variability (Fig. 2f). The highest mean values are located at the northern and southern limit of the transect and

between 51°S and 62°S, while waters around the STF (between 44 and 51°S) and in the AAR south of 62°S present values down to 300 µatm. In the CAZ, $fCO_{2sw}$ presents a strong variability, with values between 245.0 and 400.1 µatm. Besides the spatial variability, changes in $fCO_{2sw}$ can be observed at the temporal scale for a same location. The most striking pattern is the mean increase of 34.6 µatm in $fCO_{2sw}$ in the 2019 cruise compared to the period 2005–2010. A concomitant increase of 28.8 µatm is measured in the $fCO_{2atm}$ between 2005 and 2019, originating from the rise in atmospheric $CO_2$ throughout years. The highest mean increase in $fCO_{2sw}$ compared to the atmosphere could originate from the interannual variability in ocean dynamics and/or biological activity. When considering the change in $fCO_{2sw}$ with respect to $fCO_{2atm}$, the $\Delta fCO_2$ values during 2019 are closer to the ones of the years 2005–2010, highlighting that the equilibrium between atmosphere and ocean have not changed much. Mean $\Delta fCO_2$ and $FCO_2$ values range from −56.5 µatm to −4.0 µatm and from −8.0 mmol $m^{-2}$ $d^{-1}$ to −0.3 mmol $m^{-2}$ $d^{-1}$ respectively along the transect, and present similar trends to $fCO_{2sw}$ (Fig. 2g and 2). Around the STF and in the AAR south of 62°S, the surface waters are undersaturated with respect to the atmosphere, with mean values of $\Delta fCO_2$ and $FCO_2$ down to −52.0 µatm and −35.2 mmol $m^{-2}$ $d^{-1}$ respectively, defining these regions as strong sink of $CO_2$. The areas close to Tasmania coast and between 51 and 62°S show a reduced uptake in $CO_2$, with punctual $\Delta fCO_2$ higher than 0, located in the southern part of the SAR and at 61°S. The studied region is therefore a sink of $CO_2$ during the end of summer, with a mean $FCO_2$ of −4.0 ± 2.8 mmol $m^{-2}$ $d^{-1}$. The spatial distribution in air-sea exchanges in $CO_2$ have been previously observed in the region south of Tasmania over the same period of the year, with direct measurements of $fCO_2$ (Metzl et al., 1999; Brévière et al., 2006; Laika et al., 2009; Benallal et al., 2017). These studies all showed sinks of $CO_2$ north of 50°S approximately, with minimum values between 300 and 320 µatm, and $\Delta fCO_2$ down to −60 µatm. In the southern part of the SAR and northern part of the AAR, they found a smaller sink or a small source, with $\Delta fCO_2$ around 0 µatm (Brévière et al., 2006; Laika et al., 2009). In summer 2003, Brévière et al. (2006) found low $\Delta fCO_2$ (around −40 µatm), but this strong sink was concomitant with unusually strong biological activity in the area, as revealed by Chl-a concentration from satellite images. Finally, in the southern part of the AAR and in the CAZ, Laika et al. (2009) and Benallal et al. (2017) found a sink of $CO_2$ with $\Delta fCO_2$ around −40 µatm and $FCO_2$ around −4.0 ± 2.0 mmol $m^{-2}$ $d^{-1}$. The comparison of our dataset ($fCO_{2sw}$, $\Delta fCO_2$ and $FCO_2$) with the measured ones in the literature showed a very good agreement, confirming the validity of our calculated values of $fCO_{2sw}$ and $FCO_2$.

The strong sinks in $CO_2$ north of 51°S and in the AAR south of 62°S coincide with higher values of Chl-a along the transect (Fig. 2i). Satellite images of Chl-a concentrations over the weeks covered by cruises show values between 0.08 and 1.36 mg $m^{-3}$. The surface waters between 51 and 62°S are almost free of Chl-a, while north of 51°S and south of 62°S, mean weekly Chl-a values reach values up to 1 mg $m^{-3}$, still with a strong spatial and temporal variability within these areas. In the SO south of Tasmania, high biological activity is observed from austral spring to the end of austral summer, with strong phytoplankton blooms north of 50°S and south of 60°S, caused by the development of lightly silicified diatoms and coccolithophores in the north and highly silicified diatoms in the south (Balch et al., 2016; Nissen et al., 2021). Despite the difference in temporal and spatial resolution between $CO_2$ fluxes from in-situ data and Chl-a concentrations from 8-day composite satellite images, the observed decreases in $FCO_2$ towards more negative values seem to be strongly controlled by higher biological activity along the transect. Similar undersaturation of surface waters have been observed in a context of high Chl-a concentration in the SO in previous studies, confirming the direct influence of biological activity on the presence of sinks of $CO_2$ (Brévière et al., 2006; Lourantou and Metzl, 2011).

### 3.2. Processes affecting the variability of $A_T$ and $C_T$

#### 3.2.1. Drivers of $A_T$ variability

As previously seen, in the SO south of Tasmania, we observe a relationship between $A_T$ and SSS in the surface waters north of the PF. In the AAR however, $A_T$ is more related to changes in SST. Both parameters are therefore useful to calculate $A_T$ along the studied transect. Here, we determine an empirical relationship for $A_T$ using measured SSS and SST along the transect. Because most of the measurements stop before Dumont d'Urville Station, the data available in the CAZ are not sufficient to evaluate a robust relation between the parameters as well as their temporal variability. Data in the STZ are not considered either, because of the influence of the Tasmanian Coast and of the strong spatial variability of the data in the STZ. The dataset is therefore composed of a total of 1413 samples over 6 different years from 2005 to 2019 and located in the SAR and AAR.

We determined a linear dependence between $A_T$ and SSS and SST, resulting the following equation:

$$A_{T_{calc}} = 762.69\ (\pm\ 37.03) + 45.28\ (\pm\ 1.11) * SSS - 2.15\ (\pm\ 0.10) * SST \quad (3)$$

Coefficients are presented in Table 2. The difference between measured $A_T$ and calculated $A_T$ using Equ. 3, $\Delta A_T$, is −0.02 µmol $kg^{-1}$ with a root mean squared error (RMSE) of 6.71 µmol $kg^{-1}$. The simplest relationships were chosen as more complex ones did not significantly improved the fit. No major difference was observed between the calculation of $A_T$ for the two regions individually or together. Therefore, a unique equation for the area combining SAR and AAR was selected (Equation (3) and Table 2).

Empirical relationships have been previously developed to calculate $A_T$ from physical parameters in the SO, some of them being valid for the whole SO (Lee et al., 2006) while others being valid for a specific region of the SO (Metzl et al., 1999; Laika et al., 2009; Shadwick et al., 2015) (Table 3). When using these equations, considerations should also be taken on the period of time covered by the dataset used to develop the relationship as well as the parameters used – for $A_T$, equations are based on SSS only (Metzl et al., 1999; Shadwick et al., 2015) or using both SSS and SST (Lee et al., 2006; Laika et al., 2009) (Table 3). The highest bias and RSME are given by the equation of Shadwick et al. (2015) (27.0 ± 29.3 µmol $kg^{-1}$). This can be explained by several factors: first, the equation is defined from SSS only for an area close to the STF. When using this equation for the entire transect through SAR and AAR, the dependence of $A_T$ to changes in SST in the AAR is not considered, leading to important bias in the calculation of $A_T$. Moreover, the dataset used includes measurements over several seasons, while our dataset is restricted to the end of summer.

The other equations (Metzl et al., 1999; Lee et al., 2006; Laika et al., 2009) are in better agreement with the measured $A_T$. However, the error on the calculation of $A_T$ using these formulas are still greater than when using Equ. 3. In detail, Lee et al. (2006) and Laika et al. (2009) equations are based on the relationship of $A_T$ with SSS and SST. While Lee et al. (2006) equation is defined for the whole SO over all seasons, the equation used in Laika et al. (2009) is based on spring-summer measurements of year 2005–2006 along the same transect used in this study. Lee et al. (2006) calculated $A_T$ present slightly lower error compared to Laika et al. (2009). Finally, Metzl et al. (1999) propose three equations using SSS only. The shifts and RMSE on the calculation of $A_T$ are similar to the two previous formulas described when considering both SAR and AAR datasets together. However, when using Metzl et al. (1999) equations for SAR and AAR separately, the equations are a better fit in the SAR (mean shift of 4.4 ± 8.4 µmol $kg^{-1}$) than in the AAR (15.2 ± 16.6 µmol $kg^{-1}$). This confirms the need to use SST in addition to SSS in the equation of $A_T$ when considering the AAR.

The new equation developed in this study confirms a better fit with measured data compared to previously published equations, proving the

**Table 2**
Coefficients of each term of the equation of $A_T = a + b*SSS + c*SST$ and $C_T = a + b*SSS + c*SST + d*(fCO_{2atm} - 280)$.

| | Region | a (Intercept) | b (SSS) | c (SST) | d ($fCO_{2atm}$) | Δ (measured – calculated) | RMSE | $r^2$ |
|---|---|---|---|---|---|---|---|---|
| $A_T$ | SAR + AAR | 762.69 ± 37.03 | 45.28 ± 1.11 | −2.15 ± 0.10 | | −0.02 | 6.71 | 0.61 |
| $C_T$ | SAR | 1431.45 ± 103.61 | 20.68 ± 3.22 | −10.45 ± 0.50 | 0.56 ± 0.07 | 0.00 | 8.63 | 0.76 |
| | AAR | −269.74 ± 256.1 | 70.42 ± 7.52 | −6.27 ± 0.26 | 0.51 ± 0.06 | 0.25 | 8.15 | 0.62 |

**Table 3**
Equation of $A_T$ using physical parameters determined in the Southern Ocean.

| Reference | Equation | ΔAT (μmol $kg^{-1}$) | RMSE (μmol $kg^{-1}$) | Area | Period |
|---|---|---|---|---|---|
| Lee et al. (2006) | $A_T = 2305 + 52.48*(SSS-35)+2.85*(SSS-35)^2-0.49*(SST-20) +0.086*(SST-20)^2$ | 9.22 | 11.52 | 30°S - 60°S | All year |
| Shadwick et al. (2015) | $A_T = 53*SSS + 460$ | 26.96 | 29.31 | 46.8°S-142°E | Spring to Autumn |
| Laika et al. (2009) | $A_T = 434.711–2.599*SST + 54.671*SSS$ | 11.86 | 13.74 | 43°S-67°S and 140°E – 147°E | Spring-summer 2005/2006 |
| Metzl et al. (1999) | $A_T = 37.58*SSS + 998.74$ | 11.88 | 14.73 | South-West Indian Ocean (INDIGO-1) | March–April 1985 |
| | $A_T = 35.978*SSS + 1055.9$ | 9.13 | 12.47 | South-West Indian Ocean (INDIGO-3) | January–February 1987 |
| | $A_T = 38.736*SSS + 960.5$ | 10.87 | 14.02 | 45°S-67°S and 140°E – 145°E (WOCE/SR3) | August 1996 |
| This study | $A_T = 45.28*SSS – 2.15*SST + 762.69$ | −0.01 | 6.71 | 43°S-67°S and 140°E – 147°E | Mid-Febrauary to Mid-march |

interest of its use to complete the missing $A_T$ values for long-term study of $A_T$ variations during austral summer.

### 3.2.2. *Drivers of $C_T$ variability*

As described earlier, $C_T$ is linked to changes in SSS and SST in surface waters. It is also influenced by variations of biological activity, albeit to a lesser extent. Previous studies using empirical relationships to calculate $C_T$ are often based on SSS, SST and a parameter related to biological activity such as Chl-a, Oxygen concentration or nutrients (Anderson and Sarmiento, 1994; Lee et al., 2000; Lo Monaco et al., 2005; Bates et al., 2006; Sarma et al., 2006; McNeil et al., 2007; Arrigo et al., 2010; Alin et al., 2012). However, for our study, no in situ measurements of nutrient or Chl-a are available. Moreover, satellite observations of Chl-a are 8-daily or monthly means and can be missing because of the important proportion of clouds in this region. The low-resolution Chl-a dataset compared to the rapid changes in biological activity in this area and to the high-resolution measurements of SST and SSS performed every minute could result in inaccuracy in the calculation of $C_T$. For these reasons, we do not use biological activity-related parameter to calculate $C_T$ in this study. We are aware that the absence of biological activity-related parameter in the equation of $C_T$ increases the error on the calculation, in particular when considering calculated $C_T$ to estimate $fCO_{2sw}$. However, the spatial distribution of $C_T$ is not firstly related to changes in biological activity, as seen when comparing the latitudinal variation in $C_T$ and Chl-a (Fig. 3d and i), and using SSS and SST can help us retrieve the main $C_T$ signal. Finally, this equation does not aim to help reconstruct $fCO_{2sw}$ data – that are often measured in-situ – but aims to better constrain $C_T$ spatial and temporal variability in the SO based on well-measured physical parameters.

$C_T$ is also dependent of atmospheric $CO_2$ concentration, including $C_{ant}$. Over the past decades, anthropogenic emissions have risen, leading to an increase in $fCO_{2atm}$ but also $fCO_{2sw}$ (Fig. 3f). This parameter is therefore important when dealing with the evolution of $C_T$ through time. Lefèvre et al. (2021) included the year as a parameter to take into account the effect of atmospheric $CO_2$ evolution on $C_T$. Here we use $fCO_{2atm}$ instead as it resulted in reduced bias in $C_T$ calculation compared to the year. While $C_T$ is more directly related to changes in $fCO_{2sw}$ than $fCO_{2atm}$, the latter is measured at Cape Grim compared to $fCO_{2sw}$ that is calculated from $A_T$ and $C_T$. This answers the willingness to develop an equation that can be used with widespread parameters.

We developed a new simple equation for the calculation of $C_T$ using SSS, SST and $fCO_{2atm}$. We use the term ($fCO_{2atm} - 280$) in the equation to refer to the evolution of $fCO_{2atm}$ since the beginning of industrial period. Because the penetration of $CO_2$ in the ocean can be different in the SAR and AAR, we developed an equation for each region.

$$C_{T_{calc}} = a + b * SSS + c * SST + d * (fCO_{2atm} - 280) \quad (4)$$

Coefficients are presented in Table 2. $\Delta C_T$ are 0.00 ± 8.63 μmol $kg^{-1}$ and 0.25 ± 8.15 μmol $kg^{-1}$ for SAR and AAR respectively. Because the few available equations allowing to calculate $C_T$ in the surface SO use biological activity-related parameters or parameters that are not directly measured in our study (Lee et al., 2000; Laika et al., 2009), we could not compare our results with previous studies.

Using high resolution SST and SSS measured during the SURVOSTRAL cruises, when no in situ measurements of $A_T$ and $C_T$ are available, and using $fCO_{2atm}$ from Cape Grim station, $A_T$ and $C_T$ could be reconstructed during austral summer of all years from 2005 to 2019.

## 3.3. *Interannual variability south of Tasmania from 2005 to 2019*

Interannual and decadal evolution of the measured SST and SSS as well as $A_T$ and $C_T$ data over the period 2005–2019 are shown in Fig. 4 and Table 2 for the SAR and AAR. The trends are calculated using the mean value of February–March transects of each year.

### 3.3.1. *Interannual variability in the SAR*

In the SAR, SST and SSS both increased on average by 0.05 ± 0.02 °C $yr^{-1}$ and 0.02 ± 0.00 $yr^{-1}$ respectively (Table 4 and Fig. 4a and c). The surface waters south of Tasmania are influenced by the EAC, bringing salty and warm subtropical waters along the east coast of Tasmania. The volume of EAC flowing from the north depends on the wind stress curl. Over the past decades and in the context of global warming and climate change, an increase in wind stress curl have been observed in the Tasman Sea concomitant with a southward expansion of the subtropical gyre (Cai et al., 2005; Ridgway, 2007; Hill et al., 2008, 2011; Shears and Bowen, 2017), leading to a shift of the STF towards higher latitudes. No clear trend of STF shift was observed during austral summer (December

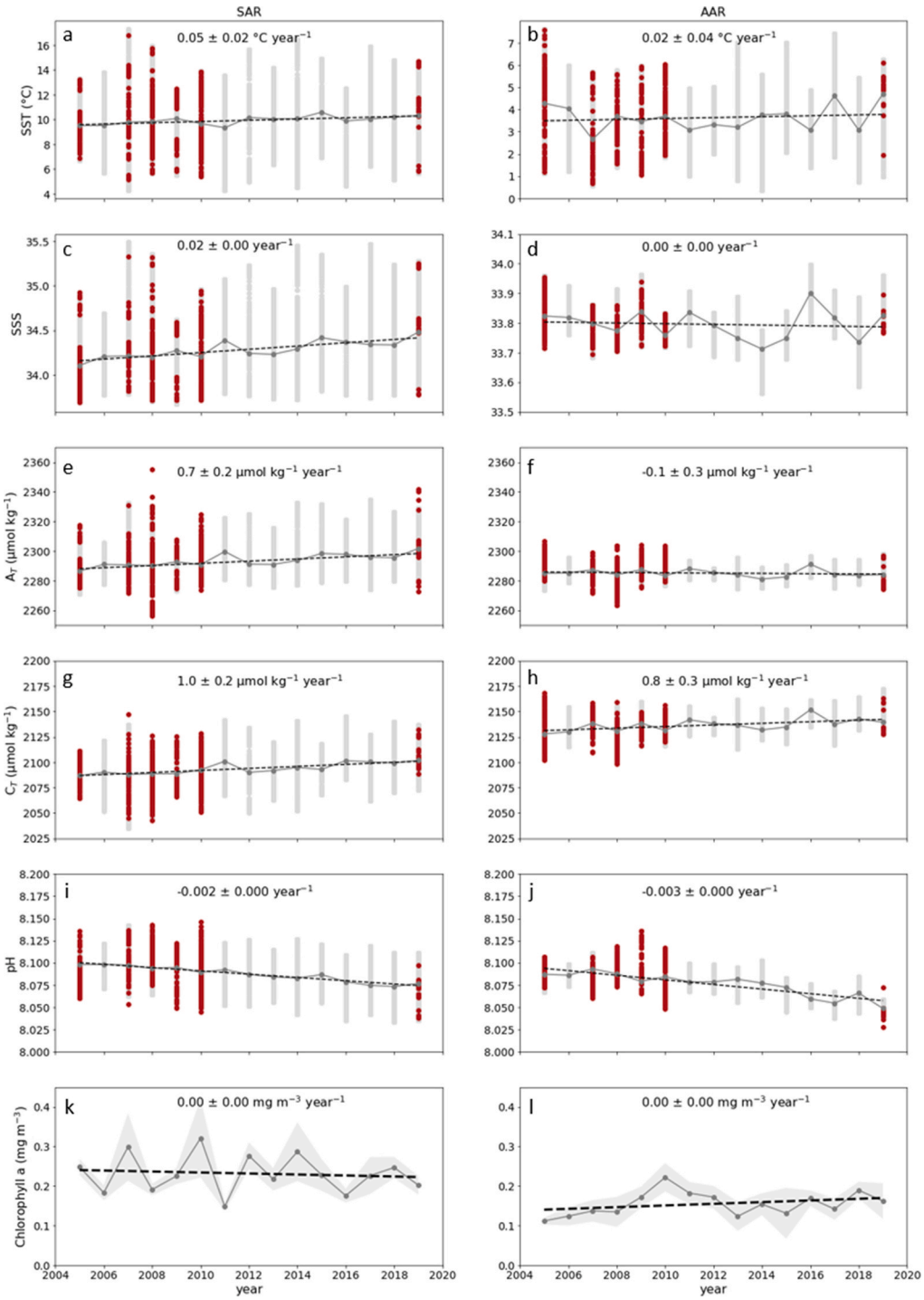



**Fig. 4.** Interannual variability of SST, SSS, $A_T$,$C_T$, pH and Chl-a from 2005 to 2019 for the SAR (a,c,e,g,I,k) and the AAR (b,d,f,h,j,l) using measured SST and SSS and calculated $A_T$ and $C_T$ from new equations developed in section 3.2 (light grey points are measured data of SST and SSS and calculated $A_T$ and $C_T$. Dark grey points are yearly mean values and black dashed line is the linear regression of the mean values for each year as a function of time. Red points are data were measured $A_T$ and $C_T$ are available. For $A_T$ and $C_T$ trends, only calculated data were used.

to March) over the 1994–2012 period on the same transect using the 13 °C isotherm from TSG SST data to define the latitude of STF (Morrow and Kestenare, 2014). However, using both the strong gradient in SSS and the 13 °C isotherm on our dataset, the position of the STF at the surface seems to migrate southward during the period 2005–2019 (Supplementary Fig. 2). The increased inputs of warm and salty subtropical waters due to southward migration of the STF could explain the increase in SST and SSS in this region. Increase in SST and SSS in other part of the SO have also been observed in relation with the poleward shift of subtropical gyres and SO fronts (Gille, 2008; Sokolov and Rintoul, 2009; Armour et al., 2016; Sallée, 2018; Yang et al., 2020). A part of the warming observed in surface waters of the SAR south of Tasmania could originate from the increasing heat uptake observed in the SO (Armour et al., 2016; Sallée, 2018; Auger et al., 2021). While some large-scale studies show a clear increase in SST in the region north of the PF in the SO, others present no clear trend, and similar observations have also been made for SSS (Midorikawa et al., 2012; Takahashi et al., 2014). However, the results may be difficult to compare depending on the period and area considered. Along the studied transect, the observed southward STF migration for the period 2005–2019 is smaller than the interannual variability. Moreover, the STF shows a strong mesoscale signature, with high variability of its position at the weekly scale, between two cruises the same year.

Reconstructed $A_T$ increases by 0.7 ± 0.2 µmol $kg^{-1}yr^{-1}$ from 2005 to

**Table 4**
Decadal trends of SST, SSS, $A_T$ and $C_T$ observed in the SAR and AAR south of Tasmania over the period 2005–2019. The trend significance is computed using Python's module statsmodels with OLS regression model (Seabold and Perktold, 2010). r is the coefficient of correlation and p-value the probability of the null hypothesis, p-value = 0.001 indicating a 100% confidence level in the trend.

| | Region | Slope | Error | r | p-value |
|---|---|---|---|---|---|
| SST (°C $yr^{-1}$) | SAR | 0.05 | 0.02 | 0.68 | 0.006 |
| | *AAR* | *0.02* | *0.04* | *0.15* | *0.58* |
| SSS ($yr^{-1}$) | SAR | 0.02 | 0.00 | 0.82 | <0.001 |
| | *AAR* | *0.00* | *0.00* | *−0.11* | *0.71* |
| AT (μmol $kg^{-1}yr^{-1}$) | SAR | 0.7 | 0.2 | 0.77 | <0.001 |
| | *AAR* | *−0.1* | *0.3* | *−0.17* | *0.18* |
| CT (μmol $kg^{-1}yr^{-1}$) | SAR | 1.0 | 0.2 | 0.82 | <0.001 |
| | *AAR* | *0.8* | *0.3* | *0.58* | *0.02* |
| pH ($yr^{-1}$) | SAR | −0.0018 | 0.0001 | −0.89 | <0.001 |
| | *AAR* | *−0.0026* | *0.0003* | *−0.96* | *<0.001* |
| Chl-a (mg $m^{-3}$ $yr^{-1}$) | SAR | 0.00 | 0.00 | −0.12 | 0.68 |
| | *AAR* | *0.00* | *0.00* | *0.32* | *0.25* |

2019 (Fig. 4e). While saltier waters tend to increase $A_T$, the increase in SST has the opposite effect. Using the coefficients of SST and SSS from $A_T$ parametrization as well as the trends in SST and SSS in the SAR, we estimate the increase in $A_T$ attributed to the rise in salinity to 0.91 ± 0.02, while the effect of SST is only −0.11 ± 0.05. The observed trend in $A_T$ is therefore primarily impacted by the change in SSS due to increasing southward flow of subtropical waters through time. Long-term evolution of $C_T$ presents an increase of 1.0 ± 0.2 μmol $kg^{-1}$ $yr^{-1}$ (Fig. 4g). The $C_T$ interannual trend is also influenced by the southward shift in subtropical waters. While the mean increase in SSS in the region also acts to increase $C_T$, the warming of surface waters reduces the $CO_2$ solubility, decreasing $C_T$. The −0.53 ± 0.24 μmol $kg^{-1}$ $yr^{-1}$ decrease in $C_T$ linked to the 0.05 ± 0.02 °C $yr^{-1}$ increasing trend in SST in the SAR would be in part compensated by the 0.42 ± 0.07 μmol $kg^{-1}$ $yr^{-1}$ rise due to the increasing trend in SSS. Moreover, biological activity variation can also affect the trend. In the SAR, interannual variability in Chl-a is observed, but the amplitude of this variability is small. No significant trend in the Chl-a concentration was observed during the period (0.00 ± 0.00 mg $m^{-3}$ $yr^{-1}$, p-value = 0.68) (Fig. 4k), confirming that the observed trend in $C_T$ is not influenced by biological activity over this period. Finally, $C_T$ is also dependent on the variability of atmospheric $CO_2$ concentration and its exchange with surface waters. The increase in atmospheric $CO_2$ explains in part the rise in $C_T$. From 2005 to 2019, the $fCO_{2atm}$ increased at a rate of 2.1 μatm $yr^{-1}$ at Cape Grim. Using the coefficient allocated to $fCO_{2atm}$-280 in the equation of $C_T$, the estimated impact of $fCO_{2atm}$ variability on $C_T$ trend is 1.18 ± 0.15 μmol $kg^{-1}$ $yr^{-1}$. At the same time, pH decreases of −0.0018 ± 0.0001 $yr^{-1}$ in the SAR (Fig. 4i). These results, along with the observed increase in $C_T$, are consistent with the surface waters response to the rise in anthropogenic $CO_2$ uptake.

### 3.3.2. *Interannual variability in the AAR*

In the AAR, SST and SSS trends are not significant between 2005 and 2019 (Table 4), however they show interannual variability, with SST and SSS amplitudes varying by up to 2 °C and 0.2 respectively around the mean (Table 4 and Fig. 4b and d). The SO SST over the past decades presents different trends between north and south of the PF. North of the PF, surface waters are warming faster than South of the PF. In the South, SST increases more slowly in the Antarctic Zone, with a cooling in the sea-ice zone in eastern Antarctica (Armour et al., 2016; Sallée, 2018; Auger et al., 2021). The absence of significant change in SST in the entire AAR during the 2005–2019 period compared to the SAR, could be explained by this north-south difference. In the AAR, as defined in this study, late-summer surface waters are influenced by the advection of freshwater from regions of sea-ice melt and also high-salinity shelf waters at the southern end from sea-ice formation, both processes leading to a strong impact on SSS (Chaigneau et al., 2004). Indeed, Morrow and Kestenare (2014) demonstrated that interannual variability in SSS was in part linked with sea-ice concentration, with years of higher sea-ice concentration in winter-spring leading to lower mean SSS the following summer, and vice versa.

As with SSS and SST, $A_T$ shows no significant trend in the AAR (p-value = 0.93) (Fig. 4f) but presents interannual variability that is related to SSS and SST variability. In contrast, $C_T$ presents a more robust trend, with a rate of 0.8 ± 0.3 μmol $kg^{-1}$ $yr^{-1}$ through the period in the AAR (p-value = 0.02) (Fig. 4h). As in the SAR, Chl-a show no significant trend in the AAR (Fig. 4l). Therefore, we conclude that the biological activity has no impact on the long-term trend in $C_T$. However, we clearly see interannual variability in the biological activity. In particular, Chl-a shows a strong peak of 0.25 mg $m^{-3}$ in 2010. In mid-February 2010, the calving of Mertz Glacier Tongue (Young et al., 2010) released multi-year, nutrient-rich sea-ice and led to increasing iron and light availability, consequently creating a diatom bloom in the area close to Antarctic Coast (Shadwick et al., 2013) and a higher biological activity in the area over the years after the event (Liniger et al., 2020). These findings could explain the slightly higher Chl-a concentration observed in the AAR after 2010 compared to the period before the calving event (Fig. 3). Because SST, SSS and Chl-a show no significant trend during the period 2005–2019, the increase in $C_T$ is likely to originate from changes in air-sea exchanges of $CO_2$. Using the same methodology as in the SAR, we estimate the influence of $fCO_{2atm}$ increase on $C_T$ of 1.07 ± 0.13 μmol $kg^{-1}$ $yr^{-1}$. Over the same period, we calculate a pH decrease of −0.0026 ± 0.0003 $yr^{-1}$ (Fig. 4j). As in the SAR, the pH trend agrees with the increase in $C_T$ observed in this region.

### 3.3.3. *Influence of anthropogenic carbon on $C_T$ and pH*

Estimates of long-term trends in $C_T$ present an increase through time in all regions of the SO; with rates between 0.4 and 1.3 μmol $kg^{-1}$ $yr^{-1}$ (Midorikawa et al., 2012; Takahashi et al., 2014; Leseurre et al., 2022). These trends reflect the combined influence of changes in $CO_2$ solubility, biological activity, oceanic circulation and in the difference between atmospheric and surface-ocean $fCO_2$ (Carroll et al., 2022). Previous studies showed that the increase in $C_T$ due to a ~2 μatm $yr^{-1}$ rise in atmospheric $pCO_2$ is around 1 ± 0.2 μmol $kg^{-1}$ $yr^{-1}$ (Bates et al., 2002, 2012; Gruber et al., 2002; Lo Monaco et al., 2021). Using the coefficient associated with $fCO_{2atm}$ in the equation of $C_T$ – and proposed here as to reflect the impact of the increase in anthropogenic carbon emissions on $C_T$, our estimates of 1.18 ± 0.14 μmol $kg^{-1}$ $yr^{-1}$ and 1.07 ± 0.13 μmol $kg^{-1}$ $yr^{-1}$ increase linked to $fCO_{2atm}$ trend in the SAR and AAR respectively are close to the expected trend. These estimates are subject to environmental uncertainty linked with the numerous mechanisms affecting $C_T$ in surface waters, as described earlier. In order to increase the confidence on $C_T$ trends and better understand the rate associated with anthropogenic emissions, observations on longer time periods are needed.

While the estimation of $C_{ant}$ long-term evolution in surface waters is difficult, the impact of increasing $C_T$ in surface waters on pH is unequivocal. In the SO, the rate of decrease in pH is estimated around 0.002 ± 0.001 $yr^{-1}$ (Midorikawa et al., 2012; Takahashi et al., 2014; Munro et al., 2015; Lauvset et al., 2015; Williams et al., 2015; Xue et al., 2018; Leseurre et al., 2022). For the period 1969–2003 in the same study area, Midorikawa et al. (2012) found a more rapid pH decrease south of the PF (−0,0020 ± 0,0003 $yr^{-1}$) than in the Subantarctic Zone and Polar Front Zone (−0,0011 ± 0,0005 and −0,0013 ± 0,0004 $yr^{-1}$ respectively). More recently, in the western part of the Indian Southern Ocean, Leseurre et al. (2022) also show higher decreasing rates of pH south of the PF compared to the PFZ for observation sites that are not under the influence of Crozet and Kerguelen islands. We observe the same difference between the AAR and SAR in our study. As proposed by Midorikawa et al. (2012), while both regions are affected by the increase in $C_{ant}$ in surface waters, the AAR is also subject to the upwelling of $C_T$-rich deep waters south of the PF. The slower decrease in pH estimated in the SAR compared to the AAR could also originate from the evolution of $A_T$

through time. While in the AAR, no significant changes in $A_T$ are observed ($-0.1 \pm 0.3$ μmol $kg^{-1}$ $yr^{-1}$), the rise in $A_T$ in the SAR ($0.7 \pm 0.2$ μmol $kg^{-1}$ $yr^{-1}$) could counteract in part the impact of increasing $C_T$ on pH. The calculated rates of pH decrease for the period 2005–2019 in both the SAR and AAR in this study are higher than those observed for the period 1969–2003 ($-0.0018 \pm 0.0001$ and $-0.0026 \pm 0.0003$ $yr^{-1}$ respectively). Similar observations have been made in the Mozambique Channel (Lo Monaco et al., 2021). This increase in the acidification rate is likely the result of the continuous increase in atmospheric $CO_2$ and is expected to further increase in the future (Jiang et al., 2019), with irreversible damages on ecosystems, in particular calcifying organisms (Doney et al., 2020).

## 4. Conclusion

The spatial and temporal variations in SST, SSS and the carbonate parameters have been explored using Mid-February to Mid-March data collected from 2005 to 2019 along a transect south of Tasmania. Latitudinal distribution of carbonate parameters reveals strong relationship with physical parameters. SST, SSS and $A_T$ show high variability in the STZ and in the northern part of the SAR impacted by the strong mesoscale activity in these areas. In the CAZ, all parameters are influenced by the freshwater fluxes from sea-ice melting. $CO_2$ parameters show that the surface waters along the transect are a sink of $CO_2$ during summer, with a mean flux of $-4.0 \pm 2.8$ mmol $m^{-2}$ $d^{-1}$. The stronger sinks are located north of 51°S (in the STZ and northern part of the SAR) and south of 62°S, including the southern part of the AAR and the CAZ. They are associated with higher biological activity compared to the area between 51°S and 62°S. Relationships between physical and carbonate parameters are used in the SAR and AAR to determine new empirical relationship for the calculation of $A_T$ and $C_T$, thus completing our dataset when no carbonate parameters are available. Using these equations, we calculated $A_T$ and $C_T$ for the period 2005–2019 in order to observe the decadal change in the surface biogeochemistry in both the SAR and AAR. In the SAR, the increase detected in SST and SSS has been linked to a southward migration of the Subtropical Front caused by the intensification of the wind stress curl and extension of the subtropical gyre north of the region. This change in hydrography also impacts $A_T$ and $C_T$ trends. $C_T$ increases by $1.0 \pm 0.2$ μmol $kg^{-1}$ $yr^{-1}$, which is attributed to the STF migration and to the increase in $fCO_{2atm}$. In the AAR, although SST, SSS and $A_T$ show no significant trends, $C_T$ increases by $0.8 \pm 0.3$ μmol $kg^{-1}$ $yr^{-1}$. The sea-surface $C_T$ increase caused by the rise in $fCO_{2atm}$ is estimated to be $1.18 \pm 0.14$ μmol $kg^{-1}$ $yr^{-1}$ and $1.07 \pm 0.13$ μmol $kg^{-1}$ $yr^{-1}$ in the SAR and AAR respectively. These estimates are close to the expected 1 μmol $kg^{-1}$ $yr^{-1}$ increase in $C_T$ linked to the +2.1 ppm $yr^{-1}$ of $CO_2$ recorded in the atmosphere during the period. Finally, the increase in $C_T$ leads to an important decrease in pH ($-0.0018 \pm 0.0001$ and $-0.0026 \pm 0.0003$ $yr^{-1}$ in the SAR and AAR respectively), implying a contribution towards ocean acidification processes and potential changes on the biogeochemistry of the ocean.

The $A_T$ and $C_T$ empirical relationships determined in this study, as well as the decadal evolution of physical and carbonate parameters in the SO bring new perspectives for the study of long-term evolution of the carbonate system. Monitoring of physical and biogeochemical parameters in the SO on regular and long-term basis are needed for a more complete study of the changes in ocean dynamics as well as carbonate and $CO_2$ systems from seasonal to decadal scales. Moreover, with the improvements of satellite observations of SST and SSS (Fine et al., 2017; Land et al., 2019), the calculation of $A_T$ and $C_T$ from empirical relationships could provide an even larger view of the carbonate system evolution in space and time.

## Declaration of competing interest

The authors declare that they have no known competing financial interests or personal relationships that could have appeared to influence the work reported in this paper.

## Data availability

Data will be made available on request.

## Acknowledgments

M. Brandon post-doctoral contract was funded by the European project ATLANTOS (grant agreement 633211). This work benefited from ICOS France project. The MINERVE program was supported by the French Institut Polaire Emile Victor (IPEV) as well as collaboration with Institut National des Sciences de l'Univers (INSU) and the CARbone AUStral Environmental Research Observatory (CARAUS). The SST and SSS data from the SURVOSTRAL program were obtained with the support of the IPEV, the ORE-SSS/LEGOS, and the CSIRO Marine and Atmospheric Research. We are grateful to Alain Poisson, who initiated the MINERVE program. We also thank Dmitry Khvorostyanov for useful discussions on data analysis. Analyses of Chl-a concentration from MODIS Aqua used in this study were downloaded from the Giovanni online data system, developed and maintained by the NASA Goddard Earth Sciences (GES) Data and Information Services Center (DISC).

## Appendix A. Supplementary data

Supplementary data to this article can be found online at https://doi.org/10.1016/j.dsr.2022.103836.

## References

Alin, S.R., Feely, R.A., Dickson, A.G., Hernández-Ayón, J.M., Juranek, L.W., Ohman, M. D., Goericke, R., 2012. Robust empirical relationships for estimating the carbonate system in the southern California Current System and application to CalCOFI hydrographic cruise data (2005-2011). J. Geophys. Res. 117, C05033 https://doi.org/10.1029/2011JC007511.

Alory, G., Delcroix, T., Téchiné, P., Diverrès, D., Varillon, D., Cravatte, S., Gouriou, Y., Grelet, J., Jacquin, S., Kestenare, É., 2015. The French contribution to the voluntary observing ships network of sea surface salinity. Deep Sea Res. Oceanogr. Res. Pap. 105, 1–18. https://doi.org/10.1016/j.dsr.2015.08.005.

Anderson, L.A., Sarmiento, J.L., 1994. Redfield ratios of remineralization determined by nutrient data analysis. Global Biogeochem. Cycles 8, 65–80. https://doi.org/10.1029/93GB03318.

Armour, K.C., Marshall, J., Scott, J.R., Donohoe, A., Newsom, E.R., 2016. Southern Ocean warming delayed by circumpolar upwelling and equatorward transport. Nat. Geosci. 9, 549–554. https://doi.org/10.1038/ngeo2731.

Arrigo, K.R., Pabi, S., van Dijken, G.L., Maslowski, W., 2010. air-sea flux of $CO_2$ in the Arctic ocean, 1998–2003. J. Geophys. Res. 115, G04024 https://doi.org/10.1029/2009JG001224.

Auger, M., Morrow, R., Kestenare, E., Sallée, J.-B., Cowley, R., 2021. Southern Ocean in-situ temperature trends over 25 years emerge from interannual variability. Nat. Commun. 12, 514. https://doi.org/10.1038/s41467-020-20781-1.

Bakker, D.C.E., Pfeil, B., Landa, C.S., Metzl, N., O'Brien, K.M., Olsen, A., Smith, K., Cosca, C., Harasawa, S., Jones, S.D., Nakaoka, S., Nojiri, Y., Schuster, U., Steinhoff, T., Sweeney, C., Takahashi, T., Tilbrook, B., Wada, C., Wanninkhof, R., Alin, S.R., Balestrini, C.F., Barbero, L., Bates, N.R., Bianchi, A.A., Bonou, F., Boutin, J., Bozec, Y., Burger, E.F., Cai, W.-J., Castle, R.D., Chen, L., Chierici, M., Currie, K., Evans, W., Featherstone, C., Feely, R.A., Fransson, A., Goyet, C., Greenwood, N., Gregor, L., Hankin, S., Hardman-Mountford, N.J., Harlay, J., Hauck, J., Hoppema, M., Humphreys, M.P., Hunt, C.W., Huss, B., Ibánhez, J.S.P., Johannessen, T., Keeling, R., Kitidis, V., Körtzinger, A., Kozyr, A., Krasakopoulou, E., Kuwata, A., Landschützer, P., Lauvset, S.K., Lefèvre, N., Lo Monaco, C., Manke, A., Mathis, J.T., Merlivat, L., Millero, F.J., Monteiro, P.M.S., Munro, D.R., Murata, A., Newberger, T., Omar, A.M., Ono, T., Paterson, K., Pearce, D., Pierrot, D., Robbins, L. L., Saito, S., Salisbury, J., Schlitzer, R., Schneider, B., Schweitzer, R., Sieger, R., Skjelvan, I., Sullivan, K.F., Sutherland, S.C., Sutton, A.J., Tadokoro, K., Telszewski, M., Tuma, M., van Heuven, S.M.A.C., Vandemark, D., Ward, B., Watson, A.J., Xu, S., 2016. A multi-decade record of high-quality $fCO_2$; data in version 3 of the Surface Ocean $CO_2$ Atlas (SOCAT). Earth Syst. Sci. Data 8, 383–413. https://doi.org/10.5194/essd-8-383-2016.

Balch, W.M., Bates, N.R., Lam, P.J., Twining, B.S., Rosengard, S.Z., Bowler, B.C., Drapeau, D.T., Garley, R., Lubelczyk, L.C., Mitchell, C., 2016. Factors regulating the great calcite belt in the Southern Ocean and its biogeochemical significance. Global Biogeochem. Cycles 30, 1124–1144. https://doi.org/10.1002/2016GB005414.

Bates, N., Astor, Y., Church, M., Currie, K., Dore, J., Gonaález-Dávila, M., Lorenzoni, L., Muller-Karger, F., Olafsson, J., Santa-Casiano, M., 2014. A time-series view of changing ocean chemistry due to ocean uptake of anthropogenic $CO_2$ and ocean acidification. oceanog 27, 126–141. https://doi.org/10.5670/oceanog.2014.16.

Bates, N.R., Best, M.H.P., Neely, K., Garley, R., Dickson, A.G., Johnson, R.J., 2012. Detecting anthropogenic carbon dioxide uptake and ocean acidification in the North Atlantic Ocean. Biogeosciences 9, 2509–2522. https://doi.org/10.5194/bg-9-2509-2012.

Bates, N.R., Pequignet, A.C., Johnson, R.J., Gruber, N., 2002. A short-term sink for atmospheric $CO_2$ in subtropical mode water of the North Atlantic Ocean. Nature 420, 489–493. https://doi.org/10.1038/nature01253.

Bates, N.R., Pequignet, A.C., Sabine, C.L., 2006. Ocean carbon cycling in the Indian Ocean: 1. Spatiotemporal variability of inorganic carbon and air-sea $CO_2$ gas exchange. Global Biogeochem. Cycles 20, GB3020. https://doi.org/10.1029/2005GB002491.

Benallal, M.A., Moussa, H., Lencina-Avila, J.M., Touratier, F., Goyet, C., El Jai, M.C., Poisson, N., Poisson, A., 2017. Satellite-derived $CO_2$ flux in the surface seawater of the Austral Ocean south of Australia. Int. J. Rem. Sens. 38, 1600–1625. https://doi.org/10.1080/01431161.2017.1286054.

Böning, C.W., Dispert, A., Visbeck, M., Rintoul, S.R., Schwarzkopf, F.U., 2008. The response of the Antarctic Circumpolar Current to recent climate change. Nat. Geosci. 1, 864–869. https://doi.org/10.1038/ngeo362.

Brévière, E., Metzl, N., Poisson, A., Tilbrook, B., 2006. Changes of the oceanic $CO_2$ sink in the eastern Indian sector of the Southern Ocean. Tellus B 58, 438–446. https://doi.org/10.1111/j.1600-0889.2006.00220.x.

Cai, W., Shi, G., Cowan, T., Bi, D., Ribbe, J., 2005. The response of the Southern Annular Mode, the East Australian Current, and the southern mid-latitude ocean circulation to global warming. Geophys. Res. Lett. 32, L23706 https://doi.org/10.1029/2005GL024701.

Carroll, D., Menemenlis, D., Dutkiewicz, S., Lauderdale, J.M., Adkins, J.F., Bowman, K. W., Brix, H., Fenty, I., Gierach, M.M., Hill, C., Jahn, O., Landschützer, P., Manizza, M., Mazloff, M.R., Miller, C.E., Schimel, D.S., Verdy, A., Whitt, D.B., Zhang, H., 2022. Attribution of space-time variability in global-ocean dissolved inorganic carbon. Global Biogeochem. Cycles 36. https://doi.org/10.1029/2021GB007162.

Carter, B.R., Feely, R.A., Wanninkhof, R., Kouketsu, S., Sonnerup, R.E., Pardo, P.C., Sabine, C.L., Johnson, G.C., Sloyan, B.M., Murata, A., Mecking, S., Tilbrook, B., Speer, K., Talley, L.D., Millero, F.J., Wijffels, S.E., Macdonald, A.M., Gruber, N., Bullister, J.L., 2019. Pacific anthropogenic carbon between 1991 and 2017. Global Biogeochem. Cycles 33, 597–617. https://doi.org/10.1029/2018GB006154.

Chaigneau, A., Morrow, R., 2002. Surface temperature and salinity variations between Tasmania and Antarctica, 1993-1999. J. Geophys. Res. 107 https://doi.org/10.1029/2001JC000808. SRF 22-1-SRF 22-8.

Chaigneau, A., Morrow, R.A., Rintoul, S.R., 2004. Seasonal and interannual evolution of the mixed layer in the Antarctic Zone south of Tasmania. Deep Sea Res. Oceanogr. Res. Pap. 51, 2047–2072. https://doi.org/10.1016/j.dsr.2004.06.013.

Chen, C.T.A., 1993. The oceanic anthropogenic $CO_2$ sink. Chemosphere 27, 1041–1064. https://doi.org/10.1016/0045-6535(93)90067-F.

Chen, C.T.A., 1982. On the distribution of anthropogenic $CO_2$ in the Atlantic and southern oceans. Deep sea Research Part A. Oceanograp. Res. Paper. 29, 563–580. https://doi.org/10.1016/0198-0149(82)90076-0.

Coatanoan, C., Goyet, C., Gruber, N., Sabine, C.L., Warner, M., 2001. Comparison of two approaches to quantify anthropogenic $CO_2$ in the ocean: results from the northern Indian Ocean. Global Biogeochem. Cycles 15, 11–25. https://doi.org/10.1029/1999GB001200.

Cresswell, G., 2000. Currents of the continental shelf and upper slope of Tasmania. In: Papers and Proceedings of the. Royal Society of Tasmania, pp. 21–30. https://doi.org/10.26749/rstpp.133.3.21.

de Lavergne, C., Palter, J.B., Galbraith, E.D., Bernardello, R., Marinov, I., 2014. Cessation of deep convection in the open Southern Ocean under anthropogenic climate change. Nat. Clim. Change 4, 278–282. https://doi.org/10.1038/nclimate2132.

DeVries, T., 2014. The oceanic anthropogenic $CO_2$ sink: storage, air-sea fluxes, and transports over the industrial era. Global Biogeochem. Cycles 28, 631–647. https://doi.org/10.1002/2013GB004739.

Dickson, A.G., 1990. Standard potential of the reaction: AgCl (s)+ 12H2 (g)= Ag (s)+ HCl (aq), and and the standard acidity constant of the ion HSO4- in synthetic sea water from 273.15 to 318.15 K. J. Chem. Therm. 22, 113–127. https://doi.org/10.1016/0021-9614(90)90074-Z.

Dickson, A.G., Millero, F.J., 1987. A comparison of the equilibrium constants for the dissociation of carbonic acid in seawater media. Deep Sea Research Part A. Oceanograp. Res. Paper. 34, 1733–1743. https://doi.org/10.1016/0198-0149(87)90021-5.

Doney, S.C., Busch, D.S., Cooley, S.R., Kroeker, K.J., 2020. The impacts of ocean acidification on marine ecosystems and reliant human communities. Annu. Rev. Environ. Resour. 45, 83–112. https://doi.org/10.1146/annurev-environ-012320-083019.

Doney, S.C., Fabry, V.J., Feely, R.A., Kleypas, J.A., 2009. ocean acidification: the other $CO_2$ problem. Ann. Rev. Mar. Sci 1, 169–192. https://doi.org/10.1146/annurev.marine.010908.163834.

Durack, P.J., Wijffels, S.E., 2010. Fifty-year trends in global ocean salinities and their relationship to broad-scale warming. J. Clim. 23, 4342–4362. https://doi.org/10.1175/2010JCLI3377.1.

Durack, P.J., Wijffels, S.E., Matear, R.J., 2012. Ocean salinities reveal strong global water cycle intensification during 1950 to 2000. Science 336, 455–458. https://doi.org/10.1126/science.1212222.

Fine, R.A., Willey, D.A., Millero, F.J., 2017. Global variability and changes in ocean total alkalinity from Aquarius satellite data. Geophys. Res. Lett. 44, 261–267. https://doi.org/10.1002/2016GL071712.

Friedlingstein, P., O'Sullivan, M., Jones, M.W., Andrew, R.M., Hauck, J., Olsen, A., Peters, G.P., Peters, W., Pongratz, J., Sitch, S., Le Quéré, C., Canadell, J.G., Ciais, P., Jackson, R.B., Alin, S., Aragão, L.E.O.C., Arneth, A., Arora, V., Bates, N.R., Becker, M., Benoit-Cattin, A., Bittig, H.C., Bopp, L., Bultan, S., Chandra, N., Chevallier, F., Chini, L.P., Evans, W., Florentie, L., Forster, P.M., Gasser, T., Gehlen, M., Gilfillan, D., Gkritzalis, T., Gregor, L., Gruber, N., Harris, I., Hartung, K., Haverd, V., Houghton, R.A., Ilyina, T., Jain, A.K., Joetzjer, E., Kadono, K., Kato, E., Kitidis, V., Korsbakken, J.I., Landschützer, P., Lefèvre, N., Lenton, A., Lienert, S., Liu, Z., Lombardozzi, D., Marland, G., Metzl, N., Munro, D.R., Nabel, J.E.M.S., Nakaoka, S.-I., Niwa, Y., O'Brien, K., Ono, T., Palmer, P.I., Pierrot, D., Poulter, B., Resplandy, L., Robertson, E., Rödenbeck, C., Schwinger, J., Séférian, R., Skjelvan, I., Smith, A.J.P., Sutton, A.J., Tanhua, T., Tans, P.P., Tian, H., Tilbrook, B., van der Werf, G., Vuichard, N., Walker, A.P., Wanninkhof, R., Watson, A.J., Willis, D., Wiltshire, A.J., Yuan, W., Yue, X., Zaehle, S., 2020. Global carbon budget 2020. Earth Syst. Sci. Data 12, 3269–3340. https://doi.org/10.5194/essd-12-3269-2020.

Fry, C.H., Tyrrell, T., Hain, M.P., Bates, N.R., Achterberg, E.P., 2015. Analysis of global surface ocean alkalinity to determine controlling processes. Mar. Chem. 174, 46–57. https://doi.org/10.1016/j.marchem.2015.05.003.

Garcia, H.E., Weathers, K.W., Paver, C.R., Smolyar, I., Boyer, T.P., Locarnini, M.M., Zweng, M.M., Mishonov, A.V., Baranova, O.K., Seidov, D., 2019. World Ocean Atlas 2018. Vol. 4: dissolved inorganic nutrients (phosphate, nitrate and nitrate+ nitrite, silicate). NOAA Atlas NESDIS 84, 35pp.

Gille, S.T., 2008. Decadal-scale temperature trends in the southern hemisphere ocean. J. Clim. 21, 4749–4765. https://doi.org/10.1175/2008JCLI2131.1.

Goyet, C., Beauverger, C., Brunet, C., Poisson, A., 1991. Distribution of carbon dioxide partial pressure in surface waters of the Southwest Indian Ocean. Tellus B 43, 1–11. https://doi.org/10.1034/j.1600-0889.1991.00001.x.

Gray, A.R., Johnson, K.S., Bushinsky, S.M., Riser, S.C., Russell, J.L., Talley, L.D., Wanninkhof, R., Williams, N.L., Sarmiento, J.L., 2018. Autonomous biogeochemical floats detect significant carbon dioxide outgassing in the high-latitude Southern Ocean. Geophys. Res. Lett. 45, 9049–9057. https://doi.org/10.1029/2018GL078013.

Gregor, Luke, Gruber, Nicolas, 2021. OceanSODA-ETHZ: a global gridded data set of the surface ocean carbonate system for seasonal to decadal studies of ocean acidification. Earth Syst. Sci. Data 13, 777–808. https://doi.org/10.5194/essd-13-777-2021.

Gruber, N., Clement, D., Carter, B.R., Feely, R.A., van Heuven, S., Hoppema, M., Ishii, M., Key, R.M., Kozyr, A., Lauvset, S.K., Lo Monaco, C., Mathis, J.T., Murata, A., Olsen, A., Perez, F.F., Sabine, C.L., Tanhua, T., Wanninkhof, R., 2019a. The oceanic sink for anthropogenic $CO_2$ from 1994 to 2007. Science 363, 1193–1199. https://doi.org/10.1126/science.aau5153.

Gruber, N., Gloor, M., Mikaloff Fletcher, S.E., Doney, S.C., Dutkiewicz, S., Follows, M.J., Gerber, M., Jacobson, A.R., Joos, F., Lindsay, K., Menemenlis, D., Mouchet, A., Müller, S.A., Sarmiento, J.L., Takahashi, T., 2009. Oceanic sources, sinks, and transport of atmospheric $CO_2$. Global Biogeochem. Cycles 23, GB1005. https://doi.org/10.1029/2008GB003349.

Gruber, N., Keeling, C.D., Bates, N.R., 2002. Interannual variability in the north Atlantic ocean carbon sink. Science 298, 2374–2378. https://doi.org/10.1126/science.1077077.

Gruber, N., Landschützer, P., Lovenduski, N.S., 2019b. The variable Southern Ocean carbon sink. Ann. Rev. Mar. Sci 11, 159–186. https://doi.org/10.1146/annurev-marine-121916-063407.

Haumann, F.A., Gruber, N., Münnich, M., Frenger, I., Kern, S., 2016. Sea-ice transport driving Southern Ocean salinity and its recent trends. Nature 537, 89–92. https://doi.org/10.1038/nature19101.

Herraiz-Borreguero, L., Rintoul, S.R., 2011. Regional circulation and its impact on upper ocean variability south of Tasmania. Deep Sea Res. Part II Top. Stud. Oceanogr. 58, 2071–2081. https://doi.org/10.1016/j.dsr2.2011.05.022.

Herraiz-Borreguero, L., Rintoul, S.R., 2010. Subantarctic Mode Water variability influenced by mesoscale eddies south of Tasmania. J. Geophys. Res.: Oceans 115. https://doi.org/10.1029/2008JC005146.

Hill, K.L., Rintoul, S.R., Coleman, R., Ridgway, K.R., 2008. Wind forced low frequency variability of the East Australia Current. Geophys. Res. Lett. 35, L08602 https://doi.org/10.1029/2007GL032912.

Hill, K.L., Rintoul, S.R., Ridgway, K.R., Oke, P.R., 2011. Decadal changes in the South Pacific western boundary current system revealed in observations and ocean state estimates. J. Geophys. Res. 116, C01009 https://doi.org/10.1029/2009JC005926.

Humphreys, M.P., Schiller, A.J., Sandborn, D.E., Gregor, L., Pierrot, D., van Heuven, S.M. A.C., Lewis, E.R., Wallace, D.W.R., 2022. PyCO2SYS: marine carbonate system calculations in Python. Zenodo. https://doi.org/10.5281/zenodo.3744275.

Jiang, L.-Q., Carter, B.R., Feely, R.A., Lauvset, S.K., Olsen, A., 2019. Surface ocean pH and buffer capacity: past, present and future. Sci. Rep. 9, 18624 https://doi.org/10.1038/s41598-019-55039-4.

Key, R.M., Kozyr, A., Sabine, C.L., Lee, K., Wanninkhof, R., Bullister, J.L., Feely, R.A., Millero, F.J., Mordy, C., Peng, T.-H., 2004. A global ocean carbon climatology: results from global data analysis project (GLODAP). Global Biogeochem. Cycles 18, GB4031. https://doi.org/10.1029/2004GB002247.

Laika, H.E., Goyet, C., Vouve, F., Poisson, A., Touratier, F., 2009. Interannual properties of the $CO_2$ system in the Southern Ocean south of Australia. Antarct. Sci. 21, 663–680. https://doi.org/10.1017/S0954102009990319.

Land, P.E., Findlay, H.S., Shutler, J.D., Ashton, I.G.C., Holding, T., Grouazel, A., Girard-Ardhuin, F., Reul, N., Piolle, J.-F., Chapron, B., Quilfen, Y., Bellerby, R.G.J., Bhadury, P., Salisbury, J., Vandemark, D., Sabia, R., 2019. Optimum satellite remote sensing of the marine carbonate system using empirical algorithms in the global ocean, the Greater Caribbean, the Amazon Plume and the Bay of Bengal. Rem. Sens. Environ. 235, 111469 https://doi.org/10.1016/j.rse.2019.111469.

Landschützer, P., Gruber, N., Haumann, F.A., Rödenbeck, C., Bakker, D.C.E., van Heuven, S., Hoppema, M., Metzl, N., Sweeney, C., Takahashi, T., Tilbrook, B.,

Wanninkhof, R., 2015. The reinvigoration of the Southern Ocean carbon sink. Science 349, 1221–1224. https://doi.org/10.1126/science.aab2620.
Lauvset, S.K., Gruber, N., Landschützer, P., Olsen, A., Tjiputra, J., 2015. Trends and drivers in global surface ocean pH over the past 3 decades. Biogeosciences 12, 1285–1298. https://doi.org/10.5194/bg-12-1285-2015.
Le Quéré, C., Rödenbeck, C., Buitenhuis, E.T., Conway, T.J., Langenfelds, R., Gomez, A., Labuschagne, C., Ramonet, M., Nakazawa, T., Metzl, N., Gillett, N., Heimann, M., 2007. Saturation of the Southern Ocean $CO_2$ sink due to recent climate change. Science 316, 1735–1738. https://doi.org/10.1126/science.1136188.
Lee, K., Tong, L.T., Millero, F.J., Sabine, C.L., Dickson, A.G., Goyet, C., Park, G.-H., Wanninkhof, R., Feely, R.A., Key, R.M., 2006. Global relationships of total alkalinity with salinity and temperature in surface waters of the world's oceans. Geophys. Res. Lett. 33, L19605 https://doi.org/10.1029/2006GL027207.
Lee, K., Wanninkhof, R., Feely, R.A., Millero, F.J., Peng, T.-H., 2000. Global relationships of total inorganic carbon with temperature and nitrate in surface seawater. Global Biogeochem. Cycles 14, 979–994. https://doi.org/10.1029/1998GB001087.
Lefèvre, N., Mejia, C., Khvorostyanov, D., Beaumont, L., Koffi, U., 2021. Ocean circulation drives the variability of the carbon system in the eastern tropical Atlantic. Oceans 2, 126–148. https://doi.org/10.3390/oceans2010008.
Lenton, A., Metzl, N., Takahashi, T., Kuchinke, M., Matear, R.J., Roy, T., Sutherland, S.C., Sweeney, C., Tilbrook, B., 2012. The observed evolution of oceanic $pCO_2$ and its drivers over the last two decades. Global Biogeochem. Cycles 26, GB2021. https://doi.org/10.1029/2011GB004095.
Lenton, A., Tilbrook, B., Law, R.M., Bakker, D., Doney, S.C., Gruber, N., Ishii, M., Hoppema, M., Lovenduski, N.S., Matear, R.J., McNeil, B.I., Metzl, N., Mikaloff Fletcher, S.E., Monteiro, P.M.S., Rödenbeck, C., Sweeney, C., Takahashi, T., 2013. Sea–air $CO_2$ fluxes in the Southern Ocean for the period 1990–2009. Biogeosciences 10, 4037–4054. https://doi.org/10.5194/bg-10-4037-2013.
Leseurre, C., Lo Monaco, C., Reverdin, G., Metzl, N., Fin, J., Mignon, C., Benito, L., 2022. Summer trends and drivers of sea surface $fCO_2$ and pH changes observed in the Southern Indian Ocean over the last two decades (1998–2019). Biogeosciences 19, 2599–2625. https://doi.org/10.5194/bg-19-2599-2022.
Lewis, E.R., Wallace, D.W.R., 1998. Program Developed for $CO_2$ System Calculations. Environmental System Science Data Infrastructure for a Virtual Ecosystem, United States.
Liniger, G., Strutton, P.G., Lannuzel, D., Moreau, S., 2020. Calving event led to changes in phytoplankton bloom phenology in the Mertz polynya, Antarctica. J. Geophys. Res.: Oceans 125, e2020JC016387. https://doi.org/10.1029/2020JC016387.
Lo Monaco, C., Goyet, C., Metzl, N., Poisson, A., Touratier, F., 2005. Distribution and inventory of anthropogenic $CO_2$ in the Southern Ocean: comparison of three data-based methods. J. Geophys. Res. 110 https://doi.org/10.1029/2004JC002571.
Lo Monaco, C., Metzl, N., Fin, J., Mignon, C., Cuet, P., Douville, E., Gehlen, M., Chau, T. T.T., Tribollet, A., 2021. Distribution and long-term change of the sea surface carbonate system in the Mozambique Channel (1963–2019). In: Deep Sea Research Part II: Topical Studies in Oceanography 186–188, 104936. https://doi.org/10.1016/j.dsr2.2021.104936.
Lourantou, A., Metzl, N., 2011. Decadal evolution of carbon sink within a strong bloom area in the subantarctic zone. Geophys. Res. Lett. 38, L23608 https://doi.org/10.1029/2011GL049614.
Lovenduski, N.S., Gruber, N., Doney, S.C., 2008. Toward a mechanistic understanding of the decadal trends in the Southern Ocean carbon sink. Global Biogeochem. Cycles 22, GB3016. https://doi.org/10.1029/2007GB003139.
Mahieu, L., Lo Monaco, C., Metzl, N., Fin, J., Mignon, C., 2020. Variability and stability of anthropogenic $CO_2$ in Antarctic bottom water observed in the Indian sector of the Southern Ocean. Ocean Sci. 16, 1559–1576. https://doi.org/10.5194/os-16-1559-2020, 1978–2018.
McNeil, B.I., Metzl, N., Key, R.M., Matear, R.J., Corbiere, A., 2007. An empirical estimate of the Southern Ocean air-sea $CO_2$ flux. Global Biogeochem. Cycles 21, GB3011. https://doi.org/10.1029/2007GB002991.
Mehrbach, C., Culberson, C.H., Hawley, J.E., Pytkowicx, R.M., 1973. Measurement of the apparent dissociation constants of carbonic acid in seawater at atmospheric pressure 1. Limnol. Oceanogr. 18, 897–907. https://doi.org/10.4319/lo.1973.18.6.0897.
Merlivat, L., Boutin, J., Antoine, D., Beaumont, L., Golbol, M., Vellucci, V., 2018. Increase of dissolved inorganic carbon and decrease in pH in near-surface waters in the Mediterranean Sea during the past two decades. Biogeosciences 15, 5653–5662. https://doi.org/10.5194/bg-15-5653-2018.
Metzl, N., 2009. Decadal increase of oceanic carbon dioxide in Southern Indian Ocean surface waters (1991–2007). Deep Sea Res. Part II Top. Stud. Oceanogr. 56, 607–619. https://doi.org/10.1016/j.dsr2.2008.12.007.
Metzl, N., Brunet, C., Jabaud-Jan, A., Poisson, A., Schauer, B., 2006. Summer and winter air–sea $CO_2$ fluxes in the Southern Ocean. Deep Sea Res. Oceanogr. Res. Pap. 53, 1548–1563. https://doi.org/10.1016/j.dsr.2006.07.006.
Metzl, N., Lo Monaco, C., Leseurre, C., Ridame, C., Fin, J., Mignon, C., Gehlen, M., Chau, T.T.T., 2022. The impact of the South-East Madagascar Bloom on the oceanic $CO_2$ sink. Biogeosciences 19, 1451–1468. https://doi.org/10.5194/bg-19-1451-2022.
Metzl, N., Poisson, A., Louanchi, F., Brunet, C., Schauer, B., Bres, B., 1995. Spatio-temporal distributions of air-sea fluxes of $CO_2$ in the Indian and Antarctic oceans. Tellus B 47, 56–69. https://doi.org/10.3402/tellusb.v47i1-2.16006.
Metzl, N., Tilbrook, B., Poisson, A., 1999. The annual $CO_2$ cycle and the air-sea $CO_2$ flux in the sub-Antarctic Ocean. Tellus B 51, 849–861. https://doi.org/10.1034/j.1600-0889.1999.t01-3-00008.x.
Midorikawa, T., Inoue, H.Y., Ishii, M., Sasano, D., Kosugi, N., Hashida, G., Nakaoka, S., Suzuki, T., 2012. Decreasing pH trend estimated from 35-year time series of carbonate parameters in the Pacific sector of the Southern Ocean in summer. Deep Sea Res. Oceanogr. Res. Pap. 61, 131–139. https://doi.org/10.1016/j.dsr.2011.12.003.
Mikaloff Fletcher, S.E., Gruber, N., Jacobson, A.R., Doney, S.C., Dutkiewicz, S., Gerber, M., Follows, M., Joos, F., Lindsay, K., Menemenlis, D., Mouchet, A., Müller, S.A., Sarmiento, J.L., 2006. Inverse estimates of anthropogenic $CO_2$ uptake, transport, and storage by the ocean. Global Biogeochem. Cycles 20, GB2002. https://doi.org/10.1029/2005GB002530.
Millero, F.J., Lee, K., Roche, M., 1998. Distribution of alkalinity in the surface waters of the major oceans. Mar. Chem. 60, 111–130. https://doi.org/10.1016/S0304-4203(97)00084-4.
Moreau, S., Penna, A.D., Llort, J., Patel, R., Langlais, C., Boyd, P.W., Matear, R.J., Phillips, H.E., Trull, T.W., Tilbrook, B., Lenton, A., Strutton, P.G., 2017. Eddy-induced carbon transport across the Antarctic circumpolar current: eddy-induced carbon transport. Global Biogeochem. Cycles 31, 1368–1386. https://doi.org/10.1002/2017GB005669.
Morrow, R., Donguy, J.-R., Chaigneau, A., Rintoul, S.R., 2004. Cold-core anomalies at the subantarctic front, south of Tasmania. Deep Sea Res. Oceanogr. Res. Pap. 51, 1417–1440. https://doi.org/10.1016/j.dsr.2004.07.005.
Morrow, R., Kestenare, E., 2017. 22-year surface salinity changes in the Seasonal Ice Zone near 140°E off Antarctica. J. Mar. Syst. 175, 46–62. https://doi.org/10.1016/j.jmarsys.2017.07.003.
Morrow, R., Kestenare, E., 2014. Nineteen-year changes in surface salinity in the Southern Ocean south of Australia. J. Mar. Syst. 129, 472–483. https://doi.org/10.1016/j.jmarsys.2013.09.011.
Munro, D.R., Lovenduski, N.S., Takahashi, T., Stephens, B.B., Newberger, T., Sweeney, C., 2015. Recent evidence for a strengthening $CO_2$ sink in the Southern Ocean from carbonate system measurements in the Drake Passage (2002–2015). Geophys. Res. Lett. 42, 7623–7630. https://doi.org/10.1002/2015GL065194.
Murata, A., Kumamoto, Y., Sasaki, K., Watanabe, S., Fukasawa, M., 2010. Decadal increases in anthropogenic CO2 along 20°S in the south Indian ocean. J. Geophys. Res. 115, C12055 https://doi.org/10.1029/2010JC006250.
Nissen, C., Gruber, N., Münnich, M., Vogt, M., 2021. Southern Ocean phytoplankton community structure as a gatekeeper for global nutrient biogeochemistry. Global Biogeochem. Cycles 35. https://doi.org/10.1029/2021GB006991.
Oliver, E.C.J., Herzfeld, M., Holbrook, N.J., 2016. Modelling the shelf circulation off eastern Tasmania. Continent. Shelf Res. 130, 14–33. https://doi.org/10.1016/j.csr.2016.10.005.
Oliver, E.C.J., Holbrook, N.J., 2018. Variability and long-term trends in the shelf circulation off eastern Tasmania. J. Geophys. Res. Oceans 123, 7366–7381. https://doi.org/10.1029/2018JC013994.
Orr, J.C., Fabry, V.J., Aumont, O., Bopp, L., Doney, S.C., Feely, R.A., Gnanadesikan, A., Gruber, N., Ishida, A., Joos, F., Key, R.M., Lindsay, K., Maier-Reimer, E., Matear, R., Monfray, P., Mouchet, A., Najjar, R.G., Plattner, G.-K., Rodgers, K.B., Sabine, C.L., Sarmiento, J.L., Schlitzer, R., Slater, R.D., Totterdell, I.J., Weirig, M.-F., Yamanaka, Y., Yool, A., 2005. Anthropogenic ocean acidification over the twenty-first century and its impact on calcifying organisms. Nature 437, 681–686. https://doi.org/10.1038/nature04095.
Orsi, A.H., Whitworth III, T., Nowlin Jr., W.D., 1995. On the meridional extent and fronts of the Antarctic Circumpolar Current. Deep Sea Res. Oceanogr. Res. Pap. 42, 641–673. https://doi.org/10.1016/0967-0637(95)00021-W.
Pardo, P.C., Tilbrook, B., Langlais, C., Trull, T.W., Rintoul, S.R., 2017. Carbon uptake and biogeochemical change in the Southern Ocean, south of Tasmania. Biogeosciences 14, 5217–5237. https://doi.org/10.5194/bg-14-5217-2017.
Park, Y.-H., Park, T., Kim, T.-W., Lee, S.-H., Hong, C.-S., Lee, J.-H., Rio, M.-H., Pujol, M.-I., Ballarotta, M., Durand, I., Provost, C., 2019. Observations of the Antarctic circumpolar current over the udintsev fracture zone, the narrowest choke point in the Southern Ocean. J. Geophys. Res. Oceans 124, 4511–4528. https://doi.org/10.1029/2019JC015024.
Peng, T.-H., Wanninkhof, R., 2010. Increase in anthropogenic $CO_2$ in the Atlantic Ocean in the last two decades. Deep Sea Res. Oceanogr. Res. Pap. 57, 755–770. https://doi.org/10.1016/j.dsr.2010.03.008.
Ridgway, K.R., 2007. Long-term trend and decadal variability of the southward penetration of the East Australian Current. Geophys. Res. Lett. 34, L13613 https://doi.org/10.1029/2007GL030393.
Sabine, C.L., Feely, R.A., Gruber, N., Key, R.M., Lee, K., Bullister, J.L., Wanninkhof, R., Wong, C.S., Wallace, D.W.R., Tilbrook, B., Millero, F.J., Peng, T.-H., Kozyr, A., Ono, T., Rios, A.F., 2004. The oceanic sink for anthropogenic $CO_2$. Science 305, 367–371. https://doi.org/10.1126/science.1097403.
Sabine, C.L., Tanhua, T., 2010. Estimation of anthropogenic $CO_2$ inventories in the ocean. Ann. Rev. Mar. Sci 2, 175–198. https://doi.org/10.1146/annurev-marine-120308-080947.
Sallée, J.-B., 2018. Southern Ocean warming. Oceanography 31. https://doi.org/10.5670/oceanog.2018.215.
Sarma, V.V.S.S., Saino, T., Sasaoka, K., Nojiri, Y., Ono, T., Ishii, M., Inoue, H.Y., Matsumoto, K., 2006. Basin-scale $pCO_2$ distribution using satellite sea surface temperature, Chl *a*, and climatological salinity in the North Pacific in spring and summer. Global Biogeochem. Cycles 20, GB3005. https://doi.org/10.1029/2005GB002594.
Seabold, S., Perktold, J., 2010. Statsmodels: econometric and statistical modeling with python. In: Proceedings of the 9th Python in Science Conference, pp. 57–61. Austin, TX.
Shadwick, E.H., Rintoul, S.R., Tilbrook, B., Williams, G.D., Young, N., Fraser, A.D., Marchant, H., Smith, J., Tamura, T., 2013. Glacier tongue calving reduced dense water formation and enhanced carbon uptake. Geophys. Res. Lett. 40, 904–909. https://doi.org/10.1002/grl.50178.

Shadwick, E.H., Trull, T.W., Tilbrook, B., Sutton, A.J., Schulz, E., Sabine, C.L., 2015. Seasonality of biological and physical controls on surface ocean $CO_2$ from hourly observations at the Southern Ocean Time Series site south of Australia. Global Biogeochem. Cycles 29, 223–238. https://doi.org/10.1002/2014GB004906.

Shears, N.T., Bowen, M.M., 2017. Half a century of coastal temperature records reveal complex warming trends in western boundary currents. Sci. Rep. 7, 14527 https://doi.org/10.1038/s41598-017-14944-2.

Sokolov, S., Rintoul, S.R., 2009. Circumpolar structure and distribution of the Antarctic Circumpolar Current fronts: 2. Variability and relationship to sea surface height. J. Geophys. Res. 114, C11019 https://doi.org/10.1029/2008JC005248.

Sokolov, S., Rintoul, S.R., 2002. Structure of Southern Ocean fronts at 140°E. J. Mar. Syst. 34 https://doi.org/10.1016/S0924-7963(02)00200-2.

Takahashi, T., Sutherland, S.C., Chipman, D.W., Goddard, J.G., Ho, C., Newberger, T., Sweeney, C., Munro, D.R., 2014. Climatological distributions of pH, $pCO_2$, total $CO_2$, alkalinity, and $CaCO_3$ saturation in the global surface ocean, and temporal changes at selected locations. Mar. Chem. 164, 95–125. https://doi.org/10.1016/j.marchem.2014.06.004.

Takahashi, T., Sutherland, S.C., Wanninkhof, R., Sweeney, C., Feely, R.A., Chipman, D. W., Hales, B., Friederich, G., Chavez, F., Sabine, C., Watson, A., Bakker, D.C.E., Schuster, U., Metzl, N., Yoshikawa-Inoue, H., Ishii, M., Midorikawa, T., Nojiri, Y., Körtzinger, A., Steinhoff, T., Hoppema, M., Olafsson, J., Arnarson, T.S., Tilbrook, B., Johannessen, T., Olsen, A., Bellerby, R., Wong, C.S., Delille, B., Bates, N.R., de Baar, H.J.W., 2009. Climatological mean and decadal change in surface ocean $pCO_2$, and net sea–air $CO_2$ flux over the global oceans. Deep Sea Res. Part II Top. Stud. Oceanogr. 56, 554–577. https://doi.org/10.1016/j.dsr2.2008.12.009.

Wanninkhof, R., 2014. Relationship between wind speed and gas exchange over the ocean revisited: gas exchange and wind speed over the ocean. Limnol Oceanogr. Methods 12, 351–362. https://doi.org/10.4319/lom.2014.12.351.

Weiss, R.F., 1974. $CO_2$ in water and seawater: the solubility of a non-ideal gas. Mar. Chem. 2 (3), 203–215.

Wentz, F.J., Scott, J., Hoffman, R., Leidner, M., Atlas, R., Ardizzone, J., 2015. Remote Sensing Systems Cross-Calibrated Multi-Platform (CCMP) 6-hourly Ocean Vector Wind Analysis Product on 0.25 Deg Grid, Version 2.0. Remote Sensing Systems, Santa Rosa, CA.

Williams, N.L., Feely, R.A., Sabine, C.L., Dickson, A.G., Swift, J.H., Talley, L.D., Russell, J.L., 2015. Quantifying anthropogenic carbon inventory changes in the Pacific sector of the Southern Ocean. Mar. Chem. 174, 147–160. https://doi.org/10.1016/j.marchem.2015.06.015.

Wu, Y., Hain, M.P., Humphreys, M.P., Hartman, S., Tyrrell, T., 2019. What drives the latitudinal gradient in open-ocean surface dissolved inorganic carbon concentration? Biogeosciences 16, 2661–2681. https://doi.org/10.5194/bg-16-2661-2019.

Xue, L., Cai, W.-J., Takahashi, T., Gao, L., Wanninkhof, R., Wei, M., Li, K., Feng, L., Yu, W., 2018. Climatic modulation of surface acidification rates through summertime wind forcing in the Southern Ocean. Nat. Commun. 9, 3240. https://doi.org/10.1038/s41467-018-05443-7.

Yang, H., Lohmann, G., Krebs-Kanzow, U., Ionita, M., Shi, X., Sidorenko, D., Gong, X., Chen, X., Gowan, E.J., 2020. Poleward shift of the major ocean gyres detected in a warming climate. Geophys. Res. Lett. 47 https://doi.org/10.1029/2019GL085868.

Young, N., Legresy, B., Coleman, R., Massom, R., 2010. Mertz Glacier tongue unhinged by giant iceberg. Aust. Antarct. Mag. 18, 19.